

# One-dimensional infinite component vector spin glass with long-range interactions

Frank Beyer,<sup>1,\*</sup> Martin Weigel,<sup>1,2,†</sup> and M. A. Moore<sup>3,‡</sup>

<sup>1</sup>*Institut für Physik, Johannes Gutenberg-Universität Mainz, Staudinger Weg 7, D-55099 Mainz, Germany*

<sup>2</sup>*Applied Mathematics Research Centre, Coventry University, Coventry, CV1 5FB, England*

<sup>3</sup>*School of Physics and Astronomy, University of Manchester, Manchester M13 9PL, UK*

(Dated: March 4, 2013)

We investigate zero and finite temperature properties of the one-dimensional spin-glass model for vector spins in the limit of an infinite number  $m$  of spin components where the interactions decay with a power,  $\sigma$ , of the distance. A diluted version of this model is also studied, but found to deviate significantly from the fully connected model. At zero temperature, defect energies are determined from the difference in ground-state energies between systems with periodic and antiperiodic boundary conditions to determine the dependence of the defect-energy exponent  $\theta$  on  $\sigma$ . A good fit to this dependence is  $\theta = \frac{3}{4} - \sigma$ . This implies that the upper critical value of  $\sigma$  is  $3/4$ , corresponding to the lower critical dimension in the  $d$ -dimensional short-range version of the model. For finite temperatures the large  $m$  saddle-point equations are solved self-consistently which gives access to the correlation function, the order parameter and the spin-glass susceptibility. Special attention is paid to the different forms of finite-size scaling effects below and above the lower critical value,  $\sigma = 5/8$ , which corresponds to the upper critical dimension 8 of the hypercubic short-range model.

PACS numbers: 75.50.Lk, 64.60.F-, 02.60.Pn

## I. INTRODUCTION

The problem of understanding the physics of spin glasses in the form of simple model systems incorporating frustration and random disorder has challenged theoretical physicists for the last forty years<sup>1</sup>. Although significant progress has been made<sup>2</sup>, predominantly through extensive numerical simulations, a number of important puzzles are still unsolved, and we do not have a clear understanding yet of the nature of the spin-glass phase and whether replica-symmetry breaking, the hallmark of the spin-glass state in mean-field theory<sup>3</sup>, carries over to systems in low dimensions  $d$ .<sup>4</sup>

Unlike the case of ferromagnets, we have currently no means of performing a well-behaved perturbative expansion of the replica-field theory of spin glasses in dimensions below their upper critical dimension  $d_u = 6$ . While this program effectively starts from the  $d = \infty$  Sherrington-Kirkpatrick (SK)<sup>5</sup> model to understand behavior in finite dimensions, an alternative approach is to consider vector spin glasses with an infinite number of spin components  $m = \infty$ , but arbitrary spatial dimension  $d$ , and extend these results in a  $1/m$  expansion to the physically more relevant cases with finite  $m$ .<sup>6</sup> This approach appears particularly suitable as the  $m = \infty$  limit implies a number of simplifications as compared to the models with finite  $m$ . Firstly, the model is replica symmetric even in the mean-field limit<sup>7</sup>, in contrast to the Ising,  $XY$  or Heisenberg spin glasses usually considered (with  $m = 1, 2$  and  $3$  spin components, respectively). Secondly, it is tractable by analytical and numerical means. For calculations at zero temperature, it turns out to be very useful that the metastability afflicting finite- $m$  spin glasses disappears<sup>8,9</sup>, making it numerically straightforward to determine ground states. At finite temperatures, the  $m \rightarrow \infty$  limit leads to saddle-

point equations which allow for the exact calculation of correlation functions of finite samples for both mean-field and non-mean-field models<sup>10</sup>.

On the other hand, the  $m = \infty$  model has peculiarities. It has been shown that the upper critical dimension,  $d_u$ , which is six for spin glasses with a finite number of spin components, is elevated to eight<sup>11</sup>. Likewise, the *lower* critical dimension at which a finite-temperature transition first occurs, appears to be also increased from that of systems with a finite number of spin components. It has been estimated from numerical studies that<sup>12,13</sup>  $d_l \approx 6$ . The mechanism of effective dimensional reduction that is at work in lifting  $d_u$  also leads to a violation of hyperscaling even below the upper critical dimension<sup>11</sup>. Finally, regarding the numerical calculations considered here, one should note that an order of limits,  $m \rightarrow \infty$  before  $N \rightarrow \infty$ , is used which is opposite to that used in field theoretic calculations<sup>11,14</sup>. Taking the infinite-component limit first might be considered the zeroth-order term in a  $1/m$  expansion around the field-theoretic calculation<sup>15</sup>.

From studies of ferromagnets it was realized many years ago<sup>16</sup> that systems with long-range, power-law interactions in low dimensions could be used to model the non-trivial critical behavior of the kind expected in short-range systems of higher dimensions. Similar observations were later made for spin glasses<sup>17,18</sup>. It was subsequently realized that such models are useful for numerical studies, as finite-size corrections, known to be strong for spin-glass systems, depend on the *linear* extension of the lattice. Hence, studying, for instance, a one-dimensional system with interactions which fall off with distance with a power  $\sigma$  allows one to access significantly larger (linear) system sizes than studying similar systems on hypercubic lattices<sup>19–21</sup>. While these first works considered Ising spin glasses, Potts<sup>22</sup> and Heisenberg<sup>23–25</sup> models have

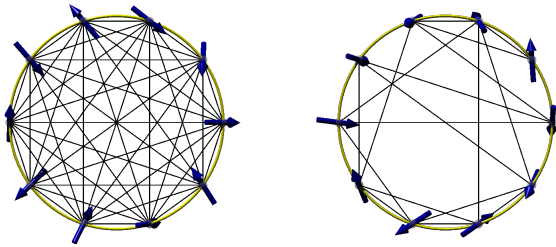


FIG. 1. (Color online). The 1d power-law spin-glass model on a ring geometry. The left panel shows the fully connected version where the magnitude of the interaction strength falls off with distance. The right panel shows the diluted model with the bond existence probability falling off with distance, whereas the bond strengths are distance independent.

also recently received some attention. For the  $m = \infty$  limit considered here, this approach appears to be well suited, as reasonable system sizes in the dimensions  $d > 6$  where a finite temperature phase transition occurs are nearly inaccessible with current computational resources. For the case of Ising spin glasses, diluted lattices have been used to reach even larger linear dimensions<sup>26–28</sup>, and the usefulness of this approach for the  $m = \infty$  model will be discussed in some detail below.

The paper is organized as follows. In Sec. II the model and some theoretical preliminaries will be introduced. Section III discusses the phase diagram of the one-dimensional spin glass with power-law interactions for finite and infinite  $m$ , and the scaling and finite-size scaling in the vicinity of the critical point. In Sec. IV, we report on the results of ground-state calculations and a study of the defect energies. The critical behavior is examined with finite-temperature methods in Sec. V. Finally, Sec. VI contains our conclusions.

## II. THE MODEL

In this paper we study flavors of the well-known Edwards-Anderson Hamiltonian

$$\mathcal{H} = -\frac{1}{2} \sum_{\substack{i,j=1 \\ i \neq j}}^L J_{ij} \mathbf{S}_i \cdot \mathbf{S}_j, \quad (1)$$

where the  $\mathbf{S}_i \in \mathbb{R}^m, i = 1, \dots, L$ , are vector spins with  $m$  components, normalized as  $|\mathbf{S}_i| = \sqrt{m}$ . The spins are organized in an effectively one-dimensional (1d) geometry, either chosen to be a chain with periodic boundary conditions or a ring as depicted in Fig. 1. In this fully connected version the exchange interactions are between all spin pairs, decaying as a power law with distance,

$$J_{ij} \sim \frac{\varphi_{ij}}{r_{ij}^\sigma}, \quad (2)$$

where  $r_{ij} = |\mathbf{r}_i - \mathbf{r}_j|$  and  $\varphi_{ij}$  is a standard normal random variable.

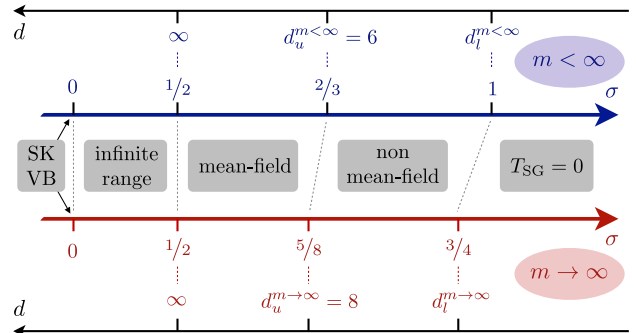


FIG. 2. (Color online). Correspondence between the 1d spin-glass model with power-law interactions characterized by an exponent  $\sigma$  and the short-range model on a hypercubic lattice of dimension  $d$ . The upper part of the figure applies to finite spin dimensions  $m$ , whereas the lower part describes the limit  $m = \infty$  discussed here. Increasing  $\sigma$  corresponds to decreasing the analogous lattice dimension  $d$ .

For the case of Ising spins ( $m = 1$ )<sup>17–20,26,27,29</sup> and, more recently, Heisenberg spins ( $m = 3$ )<sup>24,25</sup>, this model has been extensively investigated. It is found that, as the range of interactions is tuned by varying  $\sigma$ , the model has a behavior which mimics that of the short-range spin glass as its dimension  $d$  is tuned. For large  $\sigma$  the spin-glass transition temperature  $T_{SG} = 0$ . This corresponds to dimensions below the lower critical dimension  $d_l$ . A non-mean field regime is adjacent at intermediate  $\sigma$  continuing on to a mean-field region for small  $\sigma$ , which corresponds to the dimensions above the upper critical dimension,  $d_u$ . Finally the SK model<sup>5</sup> is obviously reached in the limit  $\sigma \rightarrow 0$ . The phase diagram of the model as a function of  $\sigma$  is shown in Fig. 2, and will be discussed in more detail below. A dictionary can be set up relating the behavior of the 1d power-law model at a given  $\sigma$  and a corresponding short-range model on hypercubic lattices of dimension  $d$ .<sup>26,27</sup> We shall see here that for the limit of an infinite number  $m$  of spin components, the phase diagram is modified as shown in the lower part of Fig. 2.

### A. Choice of couplings

We studied the model (1) in different variants and on different geometries.

#### Fully connected model

The fully connected system implied by Eq. (1) is realized with interaction constants

$$J_{ij} = c(\sigma, L) \frac{\varphi_{ij}}{r_{ij}^\sigma}, \quad (3)$$

where  $\varphi_{ij} \in \mathcal{N}(0, 1)$  are standard normal random variables. It is the strength of interactions that falls off as

$1/r^\sigma$  here. The mean-field transition temperature,

$$[T_{\text{SG}}^{\text{MF}}(c)]^2 = \frac{1}{L} \sum_{\substack{i,j=1 \\ i \neq j}}^L [J_{ij}^2]_{\text{av}} = \frac{c(\sigma, L)^2}{L} \sum_{\substack{i,j=1 \\ i \neq j}}^L \frac{1}{r_{ij}^{2\sigma}}, \quad (4)$$

diverges for  $\sigma \leq 1/2$ , unless we prevent this by an appropriate  $L$  dependent choice of the normalization factor  $c(\sigma, L)$ , for instance by requiring that

$$T_{\text{SG}}^{\text{MF}}(c) \stackrel{!}{=} 1, \quad (5)$$

which fixes  $c(\sigma, L)$ . While this is only strictly necessary for  $\sigma \leq 1/2$ , we apply the same normalization for all  $\sigma$ . Clearly, the limit  $\sigma \rightarrow 0$  corresponds to the SK model. In fact, it can be shown that mean-field theory is exact (at any temperature) for all  $\sigma \leq 1/2$ .<sup>30</sup> For numerical simulations employing single-spin manipulations, this fully connected model is slow as the number of bonds equals  $L(L-1)/2$ , so that the cost of a lattice sweep of updates scales quadratically with the system size  $L$ .

#### Bond-diluted model

To improve on this costly update for the fully connected model and allow numerical studies to get closer to the large system limit, a number of authors have considered a diluted version of the 1d power-law spin glass<sup>26</sup>. Its Hamiltonian reads

$$\mathcal{H} = -\frac{1}{2\sqrt{z}} \sum_{\substack{i,j=1 \\ i \neq j}}^L \varepsilon_{ij} J_{ij} \mathbf{S}_i \cdot \mathbf{S}_j, \quad (6)$$

where now  $J_{ij} \in \mathcal{N}(0, 1)$ , but the probability distribution of the dilution variables  $\varepsilon_{ij} \in \{0, 1\}$  falls off with the distance  $r_{ij}$  as

$$\varepsilon_{ij} = \begin{cases} 1, & p < p_{ij}, \\ 0, & \text{otherwise,} \end{cases} \quad (7)$$

$$p_{ij} \sim r_{ij}^{-2\sigma}, \quad (8)$$

with  $p \in \mathcal{U}[0, 1]$  a uniform random number from the interval  $[0, 1]$ . To ensure that the form of  $p_{ij}$  is a proper probability density function, we normalize<sup>27</sup>

$$p_{ij} = 1 - \exp(-A/r_{ij}^{2\sigma}), \quad (9)$$

and determine  $A$  by fixing the *average* coordination number

$$z = \sum_{i=1}^{L-1} p_{iL}. \quad (10)$$

Unless stated otherwise, for the data discussed here we used  $z = 12$ , corresponding to a hypercubic lattice at the probable lower critical dimension  $d_l = 6$ <sup>13</sup>. We apply the Newton method<sup>31</sup> in  $A$  in order to iterate the

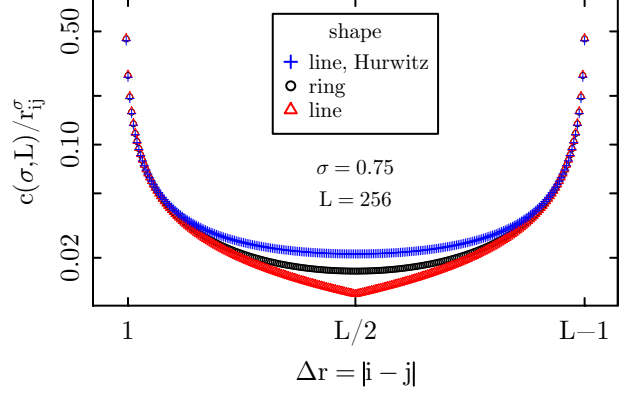


FIG. 3. (Color online). The non-random part  $c(\sigma, L)/r_{ij}^\sigma$  of the interaction constants in Eq. (3), i.e. for the fully connected model, for the line and ring geometries and the resummed (Hurwitz) version ( $\sigma = 3/4$  and  $L = 256$ ). Note the logarithmic scale of the ordinate.

probabilities  $p_{iL}$  until their sum equals the desired coordination number to a certain precision. The factor  $1/\sqrt{z}$  in Eq. (6) ensures that  $T_{\text{SG}}^{\text{MF}} = 1$ , consistent with the fully connected model. This diluted version of the model was previously studied for the Ising<sup>27</sup>, Heisenberg<sup>25</sup> and  $p$ -spin<sup>32</sup> spin-glass models. The authors of Ref. 26 and subsequent studies claimed this model to be in the same universality class as the fully connected system. As we will see below, however, this is not the case for  $\sigma > 1$ . Also, certain properties differ for  $\sigma < 1/2$ . In the limit  $\sigma \rightarrow 0$ , the diluted system corresponds to the Viana-Bray (VB) model<sup>33</sup>. Numerically, the diluted system with  $zL/2$  bonds reduces the sweep time from quadratic to linear in  $L$ .

#### B. Choice of geometry

Two different effectively one-dimensional geometries have been previously considered in studying power-law spin glasses: a ring of spins<sup>19</sup> as depicted in Fig. 1 and the possibly more natural linear chain with periodic boundary conditions without any embedding space<sup>34</sup>. In the ring model, the distances are measured according to the Euclidean metric in the plane,

$$r_{ij}^o = \frac{L}{\pi} \sin\left(\frac{\pi|i-j|}{L}\right), \quad (11)$$

and periodic boundaries are incorporated automatically. In the chain formulation, spins are located at integer positions  $i$  on a straight line with distances

$$r_{ij}^l = \min(|i-j|, L-|i-j|), \quad (12)$$

again assuming periodic boundary conditions. While one expects the specific form of the geometry to influence the finite-size behavior, in the limit of large distances on

large chains or rings, both formulations become equivalent. Universal properties, of course, should not depend on these details. On the other hand, one might argue that finite-size corrections, which are notoriously important in the study of spin-glass systems, will differ between the two formulations and might thus lead to an effective advantage for one or the other form.

When studying long-range interactions one needs to be careful about defining a controlled approach to the thermodynamic limit. Using the periodic boundary conditions preferred to suppress boundary effects, each spin effectively interacts with an infinite set of periodic images. The resulting infinite sums are usually performed in reciprocal space (Ewald summation). For the fully connected one-dimensional chain, i.e., Eq. (12), they can be performed without cut-off. Summing over images for the couplings of Eq. (3) one obtains the effective coupling

$$\begin{aligned}\tilde{J}_{ij} &= c(\sigma, L) \sqrt{\sum_{n=-\infty}^{\infty} \frac{1}{|r_{ij}^l + Ln|^{2\sigma}}} \varphi_{ij} \\ &= \frac{c(\sigma, L)}{|L|^\sigma} \sqrt{\sum_{n=-\infty}^{\infty} \frac{1}{|r_{ij}^l/L + n|^{2\sigma}}} \varphi_{ij} \\ &= \frac{c(\sigma, L)}{|L|^\sigma} \sqrt{\zeta\left(2\sigma, \frac{r_{ij}^l}{L}\right) + \zeta\left(2\sigma, 1 - \frac{r_{ij}^l}{L}\right)} \varphi_{ij},\end{aligned}\quad (13)$$

with the Hurwitz Zeta function<sup>35</sup>

$$\zeta(s, q) := \sum_{k=0}^{\infty} \frac{1}{(k+q)^s}. \quad (14)$$

The corresponding mean-field critical temperature is then

$$\begin{aligned}[T_{\text{SG}}^{\text{MF}}(c)]^2 &= \frac{1}{L} \sum_{i \neq j} [\tilde{J}_{ij}^2]_{\text{av}} = c(\sigma, L)^2 \frac{1}{|L|^{2\sigma+1}} \times \\ &\times \sum_{i \neq j} \left[ \zeta\left(2\sigma, \frac{r_{ij}^l}{L}\right) + \zeta\left(2\sigma, 1 - \frac{r_{ij}^l}{L}\right) \right],\end{aligned}\quad (15)$$

which, with the normalization  $T_{\text{SG}}^{\text{MF}}(c) = 1$ , fixes  $c(\sigma, L)$ .

While for ferromagnetic systems summation over image “charges” is crucial, for a spin-glass system with average magnetization  $\langle m \rangle = 0$  it should not change the asymptotic behavior<sup>36</sup>. It might modify finite-size corrections, however. In Fig. 3 we compare the non-random part of the interactions for the ring geometry as well as the bare and summed chain interactions. The differences away from  $r = 0$  are small and, as we shall see below, the alterations of the finite-size scaling (FSS) behavior are rather minor. Note that for the special case  $\sigma = 1$  the constants  $c(\sigma, L)$  for the ring and the summed line geometries coincide, which is easily understood from the identity<sup>35</sup>

$$\zeta\left(2, \frac{r_{ij}^l}{L}\right) + \zeta\left(2, 1 - \frac{r_{ij}^l}{L}\right) = \frac{\pi^2}{\sin^2(\pi r_{ij}^l/L)} = \left(\frac{L}{r_{ij}^o}\right)^2.$$

Unless stated otherwise, all of the calculations presented below have been performed for the ring geometry.

### III. PHASE DIAGRAM AND CRITICAL BEHAVIOR

To understand the expected critical behavior of the model in the  $m = \infty$  limit, it is useful to review and generalize the results for the  $m < \infty$  case. The most distinct feature of the  $m = \infty$  limit on hypercubic lattices is the elevation of the upper critical dimension (UCD) to  $d_u = 8$  and the accompanying violation of hyperscaling<sup>11</sup>.

#### A. Mean-field critical exponents

Recall that the mean-field exponents of (say) the Ising ferromagnet are

$$\alpha = 0, \quad \beta = 1/2, \quad \gamma = 1, \quad \nu = 1/2, \quad \eta = 0. \quad (16)$$

These satisfy hyperscaling,

$$d\nu = 2 - \alpha, \quad (17)$$

(only) at the standard upper critical dimension  $d_u = 4$ .

For the ( $m < \infty$ ) spin glass, the upper critical dimension is<sup>1</sup>  $d_u = 6$  and the mean-field value of the exponents are

$$\alpha = -1, \quad \beta = 1, \quad \gamma = 1, \quad \nu = 1/2, \quad \eta = 0. \quad (18)$$

These again satisfy hyperscaling only at the upper critical dimension,  $d_u = 6$ .  $\alpha$  and  $\beta$  are the exponents of the SK model<sup>1</sup>.

For the  $m = \infty$  spin glass the upper critical dimension is<sup>11</sup>  $d_u = 8$ . This model, however, violates hyperscaling also in the non-mean-field regime, and the hyperscaling relation is replaced by a dimensionally reduced version,

$$(d-2)\nu = 2 - \alpha. \quad (19)$$

The mean-field exponents for the  $m = \infty$  model are the same as those of the Ising spin glass i.e.

$$\alpha = -1, \quad \beta = 1, \quad \gamma = 1, \quad \nu = 1/2, \quad \eta = 0. \quad (20)$$

#### B. Finite-size scaling above the upper critical dimension

To understand the behavior of the model in the mean-field regime, it is useful to recall the relevant form of scaling and FSS above the UCD. Below the UCD, finite-size corrections depend on the ratio of correlation lengths in the finite and infinite systems,  $\xi_L/\xi_\infty \sim Lt^\nu$ , where  $t = (T - T_c)/T_c$  is the reduced temperature. For a singular quantity  $A$ , we therefore expect the FSS form<sup>37</sup>

$$A \sim L^{\kappa/\nu} \mathcal{A}(L^{1/\nu} t), \quad d < d_u, \quad (21)$$

where  $\kappa$  is the critical exponent associated to  $A$ . For a dimensionless quantity such as the finite-size correlation length normalized by the system size, we expect

$$\xi/L \sim \mathcal{X}(L^{1/\nu}t), \quad d < d_u. \quad (22)$$

At and above the UCD, FSS should hold with mean-field exponents with the role of the correlation length  $\xi_L \sim L$  taken on by some effective length<sup>38,39</sup>  $\zeta_L \sim \ell \sim N^{1/d_u} = L^{d/d_u}$ , such that

$$A \sim N^{\kappa/d_u \nu} \mathcal{A}(L^{d/d_u \nu}t), \quad d \geq d_u, \quad (23)$$

where  $\nu$  and  $\kappa$  take on their mean-field values. Similarly, for the case of a dimensionless quantity, we arrive at

$$\xi/L^{d/d_u} \sim \mathcal{X}(L^{d/d_u \nu}t), \quad d \geq d_u. \quad (24)$$

We can therefore extend the hyperscaling law beyond its usual range of validity  $d \leq d_u$  by replacing the correlation length exponent  $\nu$  with a renormalized value

$$\nu' = \begin{cases} \nu, & d < d_u, \\ d_u \nu / d = d_u / 2d, & d \geq d_u, \end{cases} \quad (25)$$

since then  $d\nu' = 2 - \alpha$  in *all* dimensions. As a consequence, at  $d = d_u$  we find

$$d\nu' = d_u/2 = 2 - \alpha, \quad (26)$$

leading to  $\alpha = 0$  for  $d_u = 4$  and  $\alpha = -1$  for  $d_u = 6$ .

Comparing the critical scaling of the Landau-Ginzburg-Wilson (GLW) effective Hamiltonian for the one-dimensional long-range model and the short-range model in general dimensions  $d$ , one infers that close to the UCD one has<sup>26</sup>

$$d_{\text{eff}} = \frac{2}{2\sigma - 1}. \quad (27)$$

As we will see below,  $\nu = 1/(2\sigma - 1) = d_{\text{eff}}/2$  in the mean-field region, such that  $d/d_u = d_{\text{eff}}/d_u = \nu/3$  and  $d/d_u \nu = 1/3$  and it follows from Eqs. (23) and (24) that

$$\chi_{\text{SG}} \sim N^{1/3} \mathcal{C}(tN^{1/3}), \quad (28a)$$

$$q_{\text{EA}} \sim N^{-1/3} \mathcal{Q}(tN^{1/3}), \quad (28b)$$

$$\frac{\xi}{L^{1/3}} \sim \mathcal{X}(tN^{1/3}). \quad (28c)$$

### C. 1d long-range spin glass

The long-range Ising spin glass was discussed analytically in Refs. 17, 18, 40, and 41. In Ref. 42 it was proven rigorously that there is no phase transition for  $\sigma > 1$ . Studying the effective GLW Hamiltonian in replica space<sup>17</sup>, it was inferred that there is a finite-temperature phase transition for  $1/2 \leq \sigma \leq 1$ , which is of mean-field type for  $1/2 \leq \sigma \leq 2/3$  and of non-mean-field type for  $2/3 < \sigma \leq 1$ . Therefore, the lower

critical  $\sigma_l = 2/3$  corresponds to the upper critical  $d_u = 6$  for systems on hypercubic lattices and similarly for the upper critical  $\sigma_u = 1$  and the lower critical  $d_l$ . It is useful to set up a dictionary of correspondences between the 1d long-range model and the short-range models on hypercubic lattices, cf. Fig. 2. Arguments were given in Larson *et al.*<sup>32</sup> that the effective dimensionality for  $2/3 \leq \sigma \leq 1$  was approximately given by<sup>27</sup>

$$d_{\text{eff}} = \frac{2 - \eta(d_{\text{eff}})}{2\sigma - 1}, \quad (29)$$

where  $\eta(d_{\text{eff}})$  is the exponent of the corresponding short-range model. The upper critical  $\sigma_u = 1$  can be inferred from the result<sup>18</sup>

$$\theta_{\text{LR}} = 1 - \sigma \quad (30)$$

for the long-range defect-energy exponent (see Sec. IV B). Since  $\theta_{\text{SR}} = -1$  for the short-range Ising spin glass in 1d, a finite-temperature transition ceases to exist at  $\theta_{\text{LR}} = 0$ , that is, at  $\sigma_u = 1$ .

In order to determine the correlation length  $\xi$  for long-range models with power-law interactions, one uses the fact that the propagator is modified from the well-known Ornstein-Zernicke form to (in reciprocal space)<sup>43,44</sup>

$$G(k) \sim \frac{1}{m^2 + k^{2\sigma-1}}. \quad (31)$$

For the spin-glass, the analogous form is for the spin-glass correlator  $\chi_{\text{SG}}(k)$ . Consequently, the second-moment definition of the correlation length is modified to

$$\xi_{\text{SG}} = \frac{1}{2 \sin(k_{\text{min}}/2)} \left[ \frac{\chi_{\text{SG}}(0)}{\chi_{\text{SG}}(\mathbf{k}_{\text{min}})} - 1 \right]^{1/(2\sigma-1)}, \quad (32)$$

with  $\mathbf{k}_{\text{min}} = (2\pi/L) \vec{e}_1 \in \mathbb{R}^d$ , where  $\vec{e}_1$  is a lattice basis vector.

At criticality (where  $m = 1/\xi = 0$ ), it is found that the Gaussian propagator  $\sim 1/k^{2\sigma-1}$  does not receive any corrections away from mean field<sup>45</sup> and hence

$$2 - \eta = 2\sigma - 1, \quad \sigma \leq 1. \quad (33)$$

The upper critical value  $\sigma_u = 1$  also follows directly from observing that at the lower critical dimension (LCD), we expect the critical correlation function decay  $G(r) \sim 1/r^{d-2+\eta}$  to be constant, i.e.,  $d_l - 2 + \eta = 0$ . Since we have  $d = 1$  and  $2 - \eta = 2\sigma - 1$ , it follows that  $\sigma_u = 1$ .

In the mean-field regime of the Ising model, Kotliar, Anderson and Stein (KAS) find<sup>17</sup>

$$\nu = 1/(2\sigma - 1), \quad 1/2 \leq \sigma \leq 2/3. \quad (34)$$

This implies that

$$\gamma = (2 - \eta)\nu = 1, \quad 1/2 \leq \sigma \leq 2/3. \quad (35)$$

Using modified hyperscaling, Eq. (26), for  $\sigma < 2/3$ , we expect

$$d\nu' = 1 \cdot \frac{1}{2\sigma - 1} \cdot \frac{6}{2/(2\sigma - 1)} = 3 \stackrel{!}{=} 2 - \alpha, \quad (36)$$

i.e.,  $\alpha = -1$  and  $\nu' = 3$  for  $1/2 \leq \sigma \leq 2/3$  and, consequently,

$$\beta = \frac{(2 - \alpha) - \gamma}{2} = 1, \quad 1/2 \leq \sigma \leq 2/3. \quad (37)$$

Note that with

$$2 - \eta = 2\sigma - 1 = (2 - \eta_{\text{MF}})/d_{\text{eff}} \quad (38)$$

and

$$\nu = \frac{1}{2\sigma - 1} = \nu_{\text{MF}} d_{\text{eff}}, \quad (39)$$

where  $d_{\text{eff}} = 2/(2\sigma - 1)$ , all exponents take their expected mean-field values.

In the non-mean-field regime,  $2/3 < \sigma < 1$ , KAS showed that an expansion around the lower critical value  $\sigma_l = 2/3$  in the variable  $\epsilon = \sigma - 2/3$  was possible and yielded to first order in  $\epsilon$

$$\frac{1}{\nu} = \frac{1}{3} - 4\epsilon. \quad (40)$$

Expansions around the upper critical  $\sigma_u = 1$  have also been proposed<sup>17,41</sup>.

#### D. 1d long-range $m = \infty$ spin glass

For the  $m = \infty$  model we know<sup>11</sup> that the UCD is elevated from the usual (spin-glass)  $d_u = 6$  to  $d_u = 8$  and that, additionally, there is a failure of hyperscaling, even below the UCD. For hypercubic lattices at the UCD, FSS should work in  $N$  (see above), e.g.,

$$\chi_{\text{SG}} \sim L^{\gamma/\nu} = L^{2-\eta} = N^{(2-\eta)/d} = N^{1/4}, \quad d \geq 8. \quad (41)$$

For the 1d long-range model, we expect the long-range form of the exponent of the correlation function, Eq. (38), to carry over to the  $m = \infty$  model. At the lower critical  $\sigma_l$ , where mean-field behavior first becomes modified, we should find

$$(2 - \eta)/d = 2 - \eta = 2\sigma_l - 1 \stackrel{!}{=} 1/4 \quad (42)$$

or  $\sigma_l = 5/8$ . Therefore, the mean-field regime is here defined as

$$1/2 \leq \sigma \leq 5/8. \quad (43)$$

Of course, this range can be also obtained directly via the calculational methods in Green *et al.*<sup>11</sup>. The effective correlation length exponent thus becomes  $\nu' = 4$  and, due to dimensional reduction, we expect a modified hyperscaling relation to hold,

$$(d - \Theta)\nu' = 2 - \alpha, \quad (44)$$

with some violation-of-hyperscaling exponent  $\Theta$  for the long-range case. Since we should have  $\alpha = -1$ , we infer

$\Theta = 1/4$  for  $1/2 \leq \sigma \leq 5/8$ . The “bare” correlation length exponent should be unaltered,

$$\nu = \frac{1}{2\sigma - 1} = \nu_{\text{MF}} d_{\text{eff}}, \quad (45)$$

so that then  $\gamma = 1$  and  $\beta = 1$  as expected from mean-field theory.

The FSS forms of the critical quantities become modified by  $d_u = 8$  according to the discussion outlined above to read

$$\chi_{\text{SG}} \sim N^{1/4} \mathcal{C}(tN^{1/4}), \quad (46a)$$

$$q_{\text{EA}} \sim N^{-1/4} \mathcal{Q}(tN^{1/4}), \quad (46b)$$

$$\frac{\xi}{L^{\nu/4}} \sim \mathcal{X}(tN^{1/4}). \quad (46c)$$

A consistent definition of the violation-of-hyperscaling exponent  $\Theta$  is given by

$$\Theta = \begin{cases} 2\sigma - 1 = 2/d_{\text{eff}}, & 5/8 \leq \sigma, \\ 1/4, & 1/2 \leq \sigma < 5/8. \end{cases} \quad (47)$$

When  $\sigma > 5/8$ , this follows from the form of the propagators at  $T_c$ , which go as  $1/k^{2\sigma-1}$ , and the results in Ref. 11.  $\Theta$  is used in scaling relations which involve the dimensionality  $d$  when one replaces  $d$  by  $d - \Theta$ . Thus the scaling relation  $\beta/\nu = (d - 2 + \eta)/2$ , with the replacements  $d \rightarrow d - \Theta$ ,  $2 - \eta = 2\sigma - 1$ , and  $d = 1$  becomes

$$\beta/\nu = (3 - 4\sigma)/2. \quad (48)$$

This is consistent with our numerical results shown in Fig. 25. It is possible to determine exactly the value of the upper critical  $\sigma_u$  from generalizing the argument that at the lower critical dimension  $d - 2 + \eta = 0$ . Replacing once again  $d \rightarrow d - \Theta$  and  $2 - \eta = 2\sigma - 1$ , one has at  $\sigma = \sigma_u$ ,  $1 - (2\sigma_u - 1) - (2\sigma_u - 1) = 3 - 4\sigma_u = 0$ , so  $\sigma_u = 3/4$ .

As will be discussed below, the defect-energy calculations for  $m = \infty$  presented here, cf. Fig. 12, can be summarized as  $\theta(\sigma = 3/4) = 0$ , i.e.,  $\sigma_u = 3/4$ , and  $\theta(\sigma = 1/2) = 1/4$ , which lead us to conjecture that

$$\theta_{\text{LR}} = \frac{3}{4} - \sigma. \quad (49)$$

In the following, we refer to  $\theta_{\text{LR}}$  simply as  $\theta$ . The form (49) works over a rather wide range of  $\sigma$ , even for  $\sigma > 3/4$  in the fully connected model. When  $\sigma > 3/4$ , there is no finite temperature transition. We have been unable to give a formal derivation of this result, but suspect that this might be possible by generalizing the formalism of Aspelmeier *et al.*<sup>46</sup> to spatially varying solutions. One can however understand Eq. (49) from the following considerations. From the scaling arguments in Ref. 18 for long-range Ising spin glasses  $2\theta = 2d - 2\sigma$ . This would also follow from the formalism of Ref. 46 which would result in an expression for the variance of the defect energy, (which scales as  $L^{2\theta}$ ) proportional to a double sum over  $i$

and  $j$  of  $[J_{ij}^2]_{\text{av}}$  if a spatially non-uniform solution for the defect energies is studied. We have to consider how the failure of hyperscaling for the large  $m$  limit might affect this relation.

$\theta$  is not a critical point exponent, but an exponent associated with the fixed point at zero temperature. For it, we suspect that the mean-field form of  $\Theta = 1/4$  is relevant for both  $\sigma$  greater than and less than  $5/8$ , since zero-temperature exponents like  $\theta$  can usually be obtained by a simple minimization of the defect energy, just as one determines mean-field behavior by minimizing the total energy of the system. Thus allowing for the failure of hyperscaling, the equation  $2\theta = 2d - 2\sigma$  becomes  $2\theta = 2(d - \Theta) - 2\sigma$ . With  $\Theta = 1/4$ , Eq. (49) for  $\theta$  is obtained on setting  $d = 1$ . We would expect this argument to still be valid in the fully connected model even for  $\sigma > 3/4$  when there is no finite temperature transition.

McMillan<sup>40,47</sup> has argued that the relevant renormalization group equation for the flow of the temperature  $T$  near the lower critical dimension is

$$\frac{dT}{d \ln L} = -\theta T + cT^3 + \dots \quad (50)$$

For  $\theta$  small and positive, (i.e., for  $\sigma$  below, but close to  $3/4$ ), one finds a fixed point at  $T_{\text{SG}} \propto \sqrt{\theta} \propto \sqrt{3 - 4\sigma}$ . If we choose the proportionality constant so that  $T_{\text{SG}}(\sigma \leq 1/2) = 1$ , then

$$T_{\text{SG}} = \sqrt{3 - 4\sigma}, \quad (51)$$

which fits the critical temperature quite well in the whole regime  $1/2 \leq \sigma \leq 3/4$  (cf. Fig. 25). The eigenvalue at this fixed point is

$$\nu = \frac{1}{2\theta} = \frac{2}{3 - 4\sigma}. \quad (52)$$

This appears to be consistent with the data shown in Fig. 23 for the regime  $5/8 \leq \sigma \leq 3/4$ , but it cannot be regarded as anything but an interpolation formula, exact only at the end points  $\sigma = 5/8$  and  $\sigma = 3/4$ . For  $\sigma > 3/4$   $T_{\text{SG}} = 0$ . Then one expects<sup>48</sup>  $\nu = -1/\theta$ .

From the scaling relation  $\gamma = \nu(2 - \eta)$  with  $\nu$  given by Eq. (52) one has the approximate result that

$$\gamma = \frac{4\sigma - 2}{3 - 4\sigma}, \quad (53)$$

in the regime  $5/8 \leq \sigma \leq 3/4$ .  $\gamma = 1$  is thus expected at  $\sigma = 5/8$  and  $\gamma \rightarrow \infty$  as  $\sigma \rightarrow 3/4$  from below.

By combining Eq. (48) with Eq. (52) one finds  $\beta = 1$  throughout the interval  $5/8 \leq \sigma \leq 3/4$ . Thus the expectation is that  $\beta$  remains close to its mean-field value even in the non-mean-field region.

#### IV. ZERO-TEMPERATURE CALCULATIONS

We start our numerical investigations of the  $m = \infty$  spin glass by studying its ground-state properties as a

function of  $\sigma$ . Due to the possibility of studying large system sizes, we first concentrated on the diluted model of Eq. (6). For most calculations, the ring arrangement was used. Compared to the ground-state problem for generic spin glasses which is found to be *NP* hard<sup>49</sup>, ground states for the  $m = \infty$  limit are much easier to determine. Starting out with the Ising model with  $m = 1$ , with increasing spin dimension the energy landscape simplifies gradually until, for  $m \rightarrow \infty$ , all metastability has vanished and the ground state becomes unique. This fact was already exploited for hypercubic systems in Ref. 13, where the lower critical dimension was determined with the defect-energy approach and for different boundary conditions.

The possibility to realize the limit  $m \rightarrow \infty$  in numerical calculations rests on the fact that for a finite system of  $N$  spins, the ground state occupies a finite dimensional sub-manifold in spin space<sup>50,51</sup>, the dimension of which is limited by the rigorous upper bound

$$m_{\text{max}}(N) = \left\lfloor \left( \sqrt{8N + 1} - 1 \right) / 2 \right\rfloor \sim N^\mu, \quad \mu = 1/2, \quad (54)$$

where  $\lfloor x \rfloor$  stands for the largest integer smaller than or equal to  $x$ . Hence, for each system size a *finite* number  $m^*(N) \leq m_{\text{max}}(N)$  of spin components is sufficient to describe the  $m = \infty$  model. For commonly used spin-glass models, the scaling is in fact weaker than  $m^*(N) \sim N^{1/2}$ . For the SK model realized, e.g., in the limit  $\sigma \rightarrow 0$  of our fully connected 1d spin glass, one finds<sup>6,50</sup>  $\mu = 2/5$ . As the degree of connectivity is lowered,  $\mu$  is reduced. We determined the required number of spin components  $m^*(N)$  for each single realization of the bonds  $J_{ij}$  and computed the disorder average  $m_0 = [m^*(N)]_{\text{av}}$ . The values of  $m^*(N)$  are found to vary only slightly between disorder realizations, such that using  $m_{\text{act}} \approx 1.1[m^*(N)]_{\text{av}}$  was sufficient to ensure that  $m = \infty$  ground states are found for all realizations. The procedure of determining the number of necessary spin dimensions  $m^*$  will be described at the end of Sec. IV A.

Due to the lack of metastability for  $m \rightarrow \infty$ , it is quite straightforward to determine true ground states numerically. Here, we employ a local spin-quench procedure, for which the spins are iteratively aligned with their respective local molecular fields  $\mathbf{H}_i$ , so that the new value of the spin  $\mathbf{S}_i$  is given by

$$\mathbf{S}'_i \parallel \mathbf{H}_i = \sum_{j \in \mathcal{N}(i)} J_{ij} \mathbf{S}_j, \quad (55)$$

where the sum runs over the set  $\mathcal{N}(i)$  of connected neighbors of the spin at site  $i$ . It is easily seen that alignment of each spin with its molecular field is a necessary condition for the system to be in its ground state. For the present case of a system without metastable states<sup>50</sup>, it is also sufficient. These updates are interspersed with sweeps of over-relaxation moves to speed up convergence, which have also been found to improve the decorrelation of systems with finite spin dimension  $m$  in Monte Carlo

simulations<sup>52</sup>. These moves, again being local, preserve the energy of the whole spin configuration since the updated spin is merely rotated around its local field and therefore moves at constant energy. The simplest way of implementing such a procedure, in particular for the case of arbitrary spin dimensions  $m$ , is to reflect the spin along  $\mathbf{H}_i$ , such that

$$\mathbf{S}'_i = -\mathbf{S}_i + 2 \frac{\mathbf{S}_i \cdot \mathbf{H}_i}{|\mathbf{H}_i|^2} \mathbf{H}_i. \quad (56)$$

This maximal movement can also be argued to lead to a maximal decorrelation effect within the constant-energy manifold of single-spin movements. The whole procedure of spin-quench and over-relaxation moves can be implemented very efficiently, since only a few elementary operations are required for each step, and no random numbers are involved.

### A. Ground-state properties

Finite-size corrections to the ground-state energy of spin glasses have been extensively discussed recently for the case of the short-range Edwards-Anderson system<sup>53–55</sup>, spin glasses on the Bethe lattice and random graphs<sup>56</sup>, and the SK model<sup>57</sup>. The dominant contribution for short-range systems is due to the presence of domain-wall defects, leading to corrections proportional to<sup>54</sup>  $L^{d-\theta}$ . For the system studied here, however, these effects, although presumably present, are masked by corrections stemming from the power-law nature of the interactions. As indicated in Eq. (4), the relevant energy scale for the case of unrenormalized coupling strengths, i. e.,  $c(\sigma, L) = 1$ , is set by the integral over the couplings,

$$\sum_{i \neq j} [J_{ij}^2]_{\text{av}} = \sum_{i=1}^{L-1} \frac{1}{r_{ij}^{2\sigma}} \sim \text{const.} + cL^{2\sigma-1}, \quad L \gg 1.$$

Hence, the ground-state energy per spin and spin-component, i. e.,  $e(L) = E/Lm$ , is expected to scale as

$$e'(L) = -\sqrt{e'_\infty{}^2 + c'L^{1-2\sigma}} + \dots, \quad (57)$$

where further finite-size corrections stemming from the presence of domain-wall excitations etc. have been neglected. We will see below that these are sub-leading and cannot be resolved by the numerics. The primed quantities in Eq. (57) are meant to indicate the unrenormalized case with  $c(\sigma, L) = 1$ . For large systems, we therefore expect different limiting behaviors depending on whether  $\sigma \gtrless 1/2$ , viz.

$$e'(L) \sim \begin{cases} e'_\infty \left( 1 + \frac{c'}{2e'_\infty{}^2} L^{1-2\sigma} \right), & \sigma > 1/2, \quad L \gg 1, \\ \sqrt{c'} L^{1/2-\sigma}, & \sigma < 1/2, \quad L \gg 1, \end{cases} \quad (58)$$

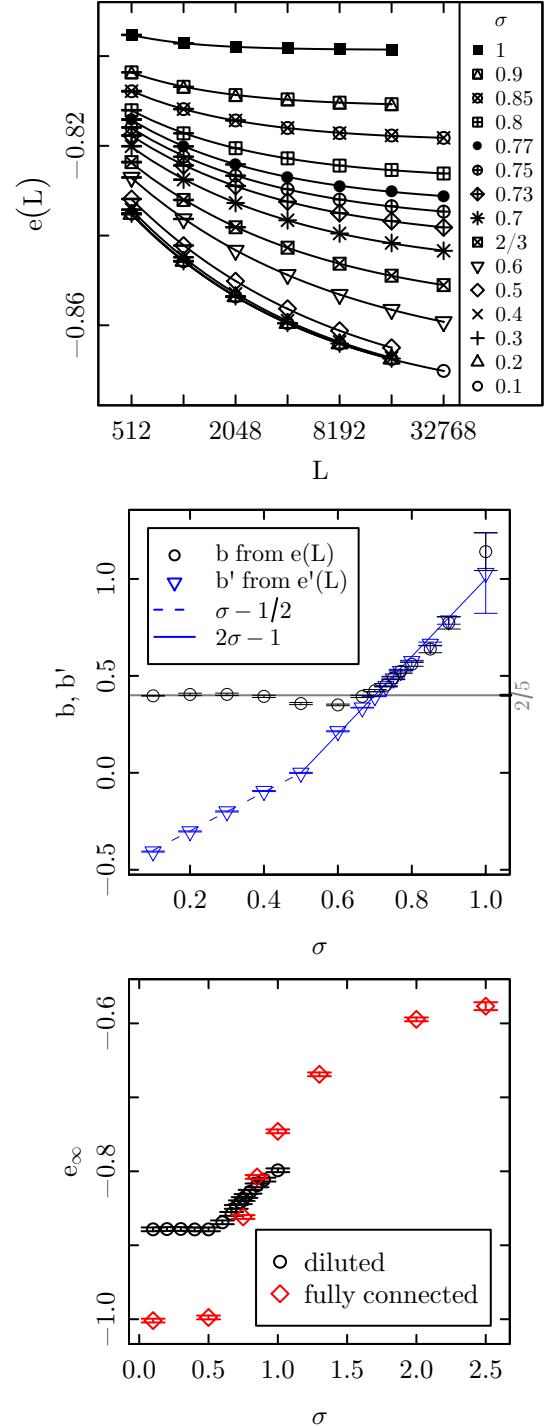


FIG. 4. (Color online). Average ground-state energies of the 1d power-law model in the  $m \rightarrow \infty$  limit. Top panel: ground-state energies  $e$  as a function of system size  $L$  and interaction range  $\sigma$ . The lines show fits of the form (61) to the data. The corresponding correction exponents  $b$  are shown in the middle panel. The blue lines indicate the expectations for the unrenormalized energies  $e'(L)$  which are  $b' = \sigma - 1/2$  for  $\sigma < 1/2$  and  $b' = 2\sigma - 1$  for  $\sigma \geq 1/2$ . The bottom panel shows the resulting asymptotic ground-state energies  $e_\infty$ , for the diluted and the fully connected model, respectively.



with logarithmic scaling right at  $\sigma = 1/2$ . If we choose to make the energy scale convergent for  $\sigma \leq 1/2$  by setting

$$c(\sigma, L)^2 = \sum_{i=1}^{L-1} \frac{1}{r_{ij}^{2\sigma}}, \quad (59)$$

we instead consider  $e(L) = e'(L) \cdot c(\sigma, L)$  with limiting behavior

$$e(L) \sim \begin{cases} e_\infty + cL^{1-2\sigma}, & \sigma > 1/2, \quad L \gg 1, \\ \text{const}, & \sigma < 1/2, \quad L \gg 1. \end{cases} \quad (60)$$

For the case of the diluted model, similar considerations lead to the same results, where now  $A$  of Eq. (9) takes on the role of  $c(\sigma, L)^2$ . In Fig. 4 we present the results of the scaling of ground-state energies. The correction exponents result from fits of the general form

$$\begin{aligned} e(L) &= e_\infty + cL^{-b}, \\ e'(L) &= e'_\infty + c'L^{-b'}, \end{aligned} \quad (61)$$

to the data. The number of disorder realizations used for the ground-state calculations are summarized in Table I. As is seen from the middle panel of Fig. 4, the predictions  $b' = 2\sigma - 1$  for  $\sigma > 1/2$  and  $b' = \sigma - 1/2$  for  $\sigma < 1/2$  for the  $e'(L)$  and  $b = 2\sigma - 1$  for  $\sigma > 1/2$  in the renormalized case are borne out well in the data. For  $\sigma < 1/2$ , where we predict  $b = 0$ , sub-leading corrections become visible. The resulting correction exponent  $b = 2/5$  is consistent with the expectations for the SK model, cf. Ref. 58 and the discussion in Sec. VD below. For the renormalized energies  $e(L)$ , we see a dip of the correction exponent for  $0.5 \leq \sigma \lesssim 0.6$ , which is possibly due to additional finite-size effects resulting from the crossover between the forms for  $\sigma \gtrless 1/2$ . As shown in the bottom panel of Fig. 4, the asymptotic ground-state energy  $e_\infty$  smoothly increases for interaction ranges  $\sigma > 1/2$ . For  $\sigma \leq 1/2$  it is independent of  $\sigma$  and takes the value  $-1$  in the fully connected version of the model<sup>8</sup>. The independence of this non-universal quantity on  $\sigma$  in this regime is a clear sign of the exactness of mean-field theory for  $\sigma \leq 1/2$  as proposed in Ref. 30. For models of lower connectivity, however, this energy is increased. Calculations on a Bethe lattice<sup>58</sup> are consistent with our results, for instance  $e_\infty(\sigma = 0.1) = -0.8784(1)$ , if the average coordination number is taken into account.

At  $T = 0$  the free energy  $F$  reduces to the internal energy. We can use this fact to consider its sample-to-sample fluctuations,

$$\sigma_N \sim N^{\Theta_f} \quad (62)$$

in a FSS analysis. The scaling of this quantity has been the subject of a number of recent analytical and numerical studies see, e.g., Refs. 53, 59–63. For the ( $m = 1$ ) Ising SK model, there has been some debate as to whether<sup>64</sup>  $\Theta_f = 1/6$  or<sup>46</sup>  $\Theta_f = 1/4$ , but now there is growing consensus that<sup>57</sup>  $\Theta_f = 1/6$ . For the  $m = \infty$  model discussed here, the situation is less well

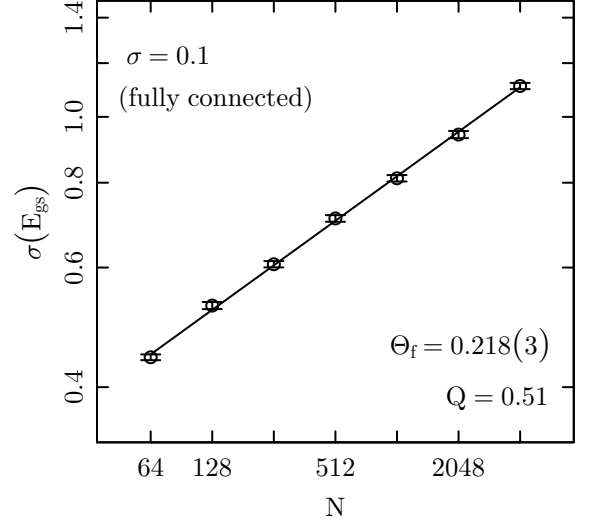


FIG. 5. The scaling behavior of the sample-to-sample fluctuations characterized by the exponent  $\Theta_f$  for  $\sigma = 0.1$ . This showcase example for the fully connected model indicates the correctness of the prediction  $\Theta_f = 1/5$  in the SK limit ( $\sigma \rightarrow 0$ ).

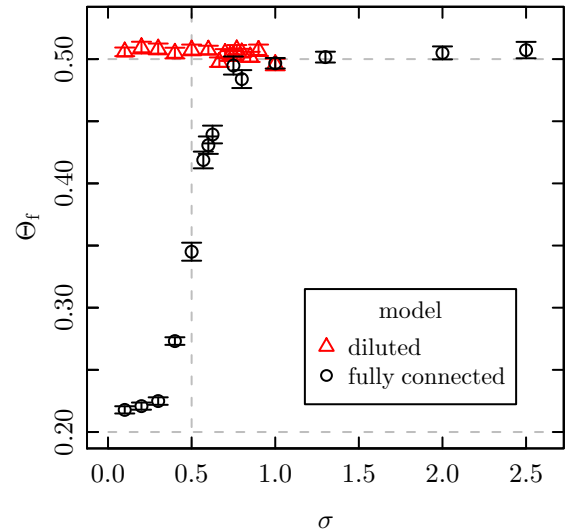


FIG. 6. (Color online). Sample-to-sample fluctuations differ for the diluted and the fully connected model. Whereas the characteristic exponent is fixed to  $1/2$  for the diluted model, it has a jump from  $1/5$  to  $1/2$  when changing from  $\sigma < 1/2$  to  $\sigma > 1/2$  for the fully connected model.

studied. For the replica symmetric spherical SK model it was shown<sup>59</sup> that  $\Theta_f = 1/3$ . As the  $m = \infty$  limit is also replica symmetric<sup>7</sup>, one might suspect this value to carry over to the present case. In Ref. 63, however, it was argued on the basis of connections of the problem to bond chaos that, instead,  $\Theta_f = 1/5$ . For the long-range model studied here, we therefore expect  $\Theta_f = 1/5$  in the

infinite-range regime  $\sigma \leq 1/2$  and a trivial  $\Theta_f = 1/2$  for  $\sigma > 1/2$ . Using our data for the ground-state energies to study this problem, we find clear power-law scaling of the distribution widths  $\sigma_N$  irrespective of the chosen value of  $\sigma$ . An example is presented in Fig. 5 for  $\sigma = 0.1$ . As shown in Fig. 6, the value of  $\Theta_f$  for the fully connected model is found to approach  $\Theta_f = 1/5$  in the SK limit as predicted, hence confirming that the  $m = \infty$  model is not in the same universality class as the spherical spin-glass. In the short-range limit  $\sigma \rightarrow \infty$ , we arrive at a trivial  $\Theta_f = 1/2$ . The transition between these two extremes, expected to be sharp at  $\sigma = 1/2$  in the thermodynamic limit, is found to be rather smeared out, however, indicating the presence of strong corrections to scaling. In contrast, the situation for the diluted model is found to be rather different with the fluctuation exponent being compatible with  $\Theta_f = 1/2$  irrespective of  $\sigma$ , cf. Fig. 6. This is some first evidence of a lack of universality between the fully connected and diluted versions of the 1d power-law model. In fact, a similar behavior was predicted in Ref. 62 for the case of diluted Ising systems, where it was attributed to the local heterogeneities caused by the fluctuating coordination number.

We also checked the distribution functions of the ground-state energies for the diluted as well as the fully connected model and each power-law exponent  $\sigma$ . While these show a non-trivial form for the (Ising) SK model<sup>60</sup>, Gaussian distributions have been reported for short-range models<sup>53</sup>. For the 1d Ising power-law chain, a crossover from Gaussian to non-trivial has been found on moving into the mean-field regime<sup>20</sup>. The distribution of ground-state energies for the 1d  $m = \infty$  model is analyzed in Fig. 7. For all values of the power-law exponent  $\sigma$  considered here ( $0.1 \leq \sigma \leq 1$ ) the distributions seem to be compatible with a Gaussian. This is indicated by a showcase example for  $\sigma = 0.1$  and  $N = 32\,678$  with a quantile-quantile plot as well as an analysis of the skewness of the distribution, estimated by

$$\hat{\gamma}_1(E) = \frac{1}{N_s} \sum_{i=1}^{N_s} \left( \frac{E_i - \hat{E}}{\hat{\sigma}_E} \right)^3 \quad (63)$$

in dependence of the system size for several values of  $\sigma$  spanning the mean-field as well as non-mean-field regimes. Here,  $N_s$  denotes the number of disorder realizations.  $\hat{E} = (1/N_s) \sum_{j=1}^{N_s} E_j$  is the usual estimator for the expectation value  $\langle E \rangle$  and  $\hat{\sigma}_E^2 = (1/(N_s - 1)) \sum_{j=1}^{N_s} (E_j - \hat{E})^2$  estimates the variance  $\sigma_E^2$ . Comparing to the results of Ref. 20, it is worthwhile to note that lattice sizes used there were considerably smaller ( $L \leq 192$ ) due to the fact that a Monte Carlo simulation was employed on the *fully connected* 1d power-law model. As shown in the lower panel of Fig. 7 for such small systems we see a significant decay for increasing lattice size similar to the one reported in Ref. 20. The data shown stem from calculations using the diluted version of the model. We also checked the fully connected version, however, and found

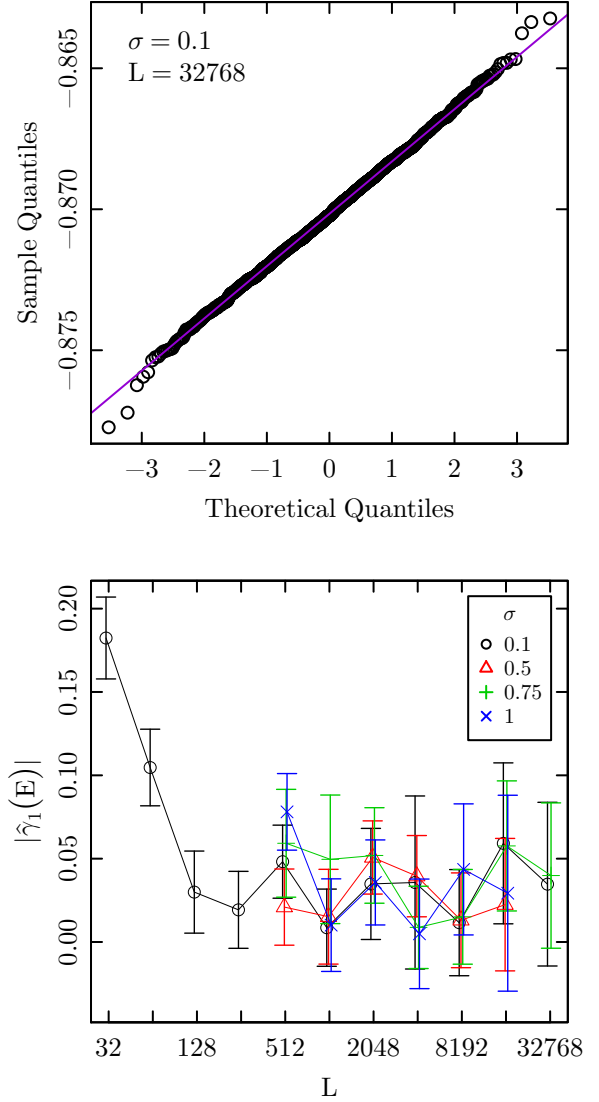


FIG. 7. (Color online). Evidence of the Gaussian nature of the ground-state energy distribution for a range of different values of  $\sigma$ . The top panel shows a normal quantile-quantile plot in a showcase example for  $\sigma = 0.1$  and the largest available lattice size  $N = 32\,678$ . Sample quantiles do not deviate from the theoretical straight line assuming a Gaussian distribution function. The lower panel shows the scaling of the (modulus of the) skewness according to Eq. (63) for  $\sigma = 0.1, 0.5, 0.75$ , and  $1$ . It vanishes for all  $\sigma$  verifying the Gaussian.

identical results (not shown).

For the case of the  $m = \infty$  model considered here another zero-temperature property concerns the average number  $m_0 = [m^*]_{\text{av}}$  of spin components required to form the ground state. We determine  $m^*$  for each realization by ordering all spin vectors of the ground state configuration into an  $m \times N$ -matrix  $M = \{\mathbf{S}_1, \dots, \mathbf{S}_N\}$  and performing a singular value decomposition (SVD) in order to calculate the number of non-zero singular values,

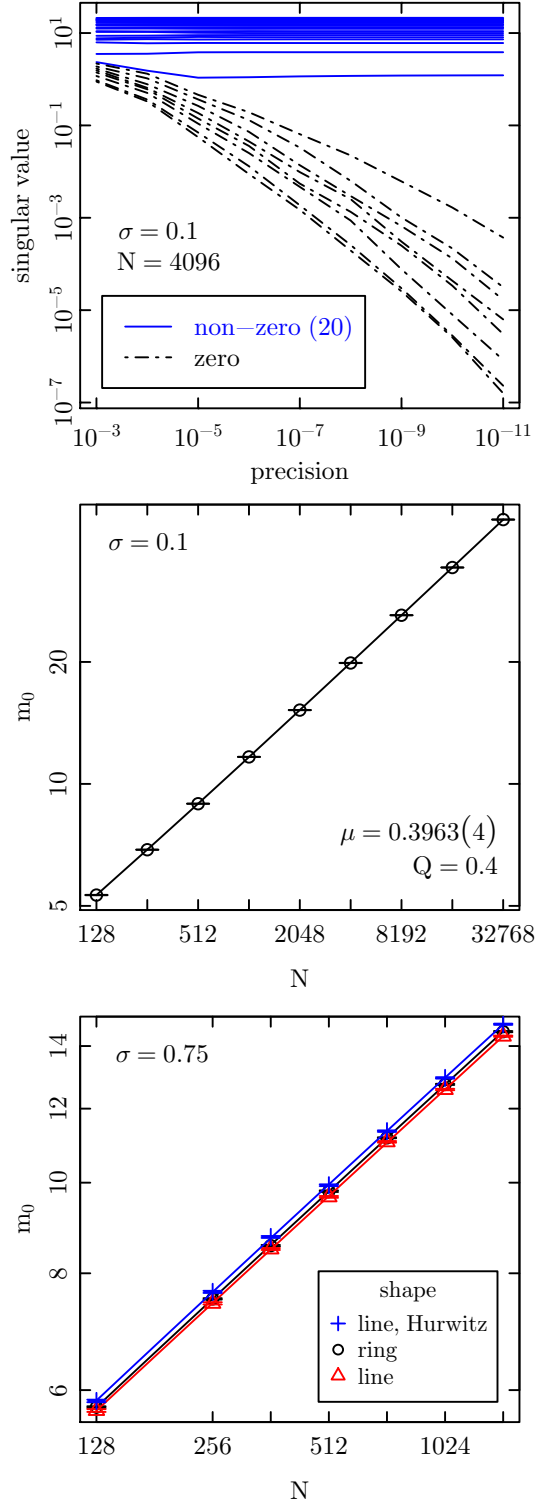


FIG. 8. (Color online). Top panel: singular values of the spin matrix  $M$  for a sample with  $N = 4096$ ,  $\sigma = 0.1$  for a quench into the ground state. The “precision” refers to the relative change of the configurational energy after a fixed number of sweeps. Middle panel: average number of ground-state spin dimensions  $m_0$  for  $\sigma = 0.1$ . The line shows a fit of the form (64) to the data. Bottom panel: comparison of  $m_0$  for the ring geometry and the line geometry with bare and resummed interactions (Hurwitz) for  $\sigma = 3/4$ .

which is equal to the rank of the matrix. Since the rank of a matrix determines the number of linearly independent columns, i.e., spin-vectors, it is the desired number  $m^*$ . In practice, we monitor the size of all singular values of  $M$  online as the quench into the ground state proceeds. As the precision of the ground-state determination is increased, those singular values that vanish in the exact ground state will scale to zero, whereas all the other singular values reach finite limiting values. This is illustrated for a sample of size  $N = 4096$  and  $\sigma = 0.1$  in the top panel of Fig. 8.

For the average number of spin components in the ground state, we assume the scaling form

$$m_0 = [m^*]_{\text{av}} = \text{const.} \times N^\mu + c, \quad (64)$$

where the additive correction  $c$  can account for the fact that for small systems  $m_0$  will not scale to zero, but will be  $m_0 = 1$  for tiny systems with  $N = 1$  and  $N = 2$ . We present the results of this analysis for the infinite-range value  $\sigma = 0.1$  and the diluted model in the middle panel of Fig. 8. Since mean-field theory is exact there, we expect to see the value  $\mu = 2/5$  found for the SK model<sup>6,50</sup>, which is indeed borne out rather well. For  $\sigma > 1/2$ ,  $\mu$  continuously decreases below  $\mu = 2/5$ , cf. the summary of our data for the diluted model in Fig. 9. A fit to a parabola yields  $\mu(\sigma) = 0.3995 - 0.55(\sigma - 0.504)^2$ . Note that since  $m_0 \sim N^\mu$  and due to the boundedness of  $\mu \leq 2/5 < 1$ , it follows that  $m_0/N \sim N^{\mu-1} \rightarrow 0$  in the thermodynamic limit. Hence, as  $T \rightarrow 0$  the spins condense into a subspace of vanishing relative size, just as in the more familiar Bose-Einstein condensation<sup>6</sup>.

To check for the influence of the different geometries introduced above in Sec. II B on the scaling results, we performed some calculations for the bare and resummed line geometries. The effect of these changes on  $m_0$  is illustrated for  $\sigma = 3/4$ , where we expect the largest deviations, in the bottom panel of Fig. 8. We find a small overall shift in  $m_0$  but, as expected, no change in  $\mu$ . Moreover, there appear to be no significant alterations of corrections to the leading FSS behavior.

## B. Defect energies

The defect-energy approach<sup>65</sup> is widely used in studying systems with spin-glass phases. It is based on the assumption that the cost  $E_{\text{def}}$  of the insertion of a system-size defect into a state of the ordered phase scales as<sup>66</sup>

$$E_{\text{def}} \propto L^\theta, \quad (65)$$

where  $\theta$  is known as the spin-stiffness exponent. Generalizing Peierls’ argument for the stability of the ordered phase of a ferromagnet, one predicts  $T_{\text{SG}} = 0$  whenever  $\theta < 0$ , whereas the ordered phase is stable at finite temperatures for  $\theta > 0$ . The limiting case  $\theta = 0$  corresponds to the LCD of the system. Additionally, for the case  $\theta < 0$  with a zero-temperature transition,  $\theta$  is related to the correlation length exponent as<sup>66</sup>  $\nu = -1/\theta$ .

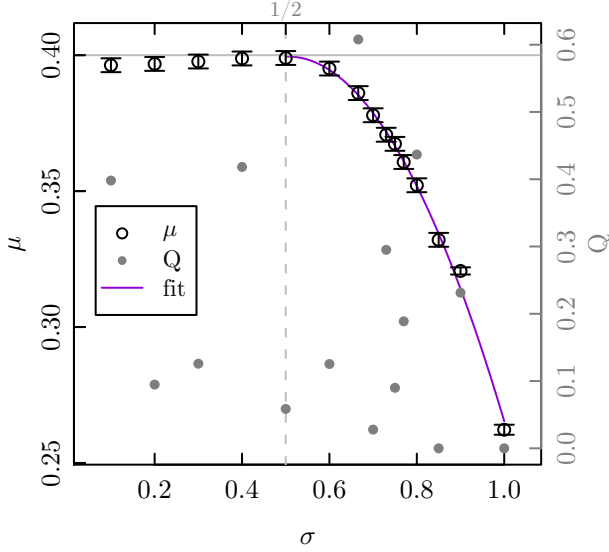


FIG. 9. (Color online). Variation of the exponent  $\mu$  with the interaction range  $\sigma$ . The points are results of fits of the form Eq. (64) to the data for the average number of occupied spin components in the ground state for the diluted version of the model. Gray full points show the quality-of-fit parameter  $Q$  (right scale). The purple line corresponds to the functional form  $\mu(\sigma) = 0.3995 - 0.55(\sigma - 0.504)^2$ .

Numerically, defect energies are conventionally determined by comparing ground states of systems with a pair of different boundary conditions (BCs) chosen such that the respective ground states must differ by a relative domain-wall type excitation. Then the defect energy corresponds to the energy difference. The most commonly used set of such BCs are periodic and antiperiodic boundaries. The defect energy of a given realization is then

$$\Delta E = |E_{AP} - E_P|, \quad (66)$$

where the modulus is required since, for symmetric coupling distributions, the two boundary conditions are statistically equivalent. For the case of the long-range ring geometry considered here, a ground-state search is performed for the original coupling configuration, yielding  $E_P$ . In the second step, the boundary exchange couplings are flipped to the antiperiodic state by choosing *one arbitrary* nearest-neighbor pair  $(\mathbf{S}_a, \mathbf{S}_{a+1})$ ,  $a \in 1, \dots, N$  (without having them necessarily interact in the diluted version of the model) and changing the sign of all interaction constants  $J_{ij}$  between spin  $\mathbf{S}_i$  and  $\mathbf{S}_j$  for all  $i \neq j$  if the shorter path between those two spins falls on top of the path between  $\mathbf{S}_a$  and  $\mathbf{S}_{a+1}$ .<sup>19</sup> A second ground-state search for this altered configuration then yields  $E_{AP}$ . There has been some discussion in the past about whether this setup is suitable for the case of continuous spins, since both periodic and antiperiodic boundaries induce some defects, such that the energy difference  $E_P - E_{AP}$  does not directly correspond to a defect energy<sup>13,67–69</sup>. Therefore, boundary conditions that

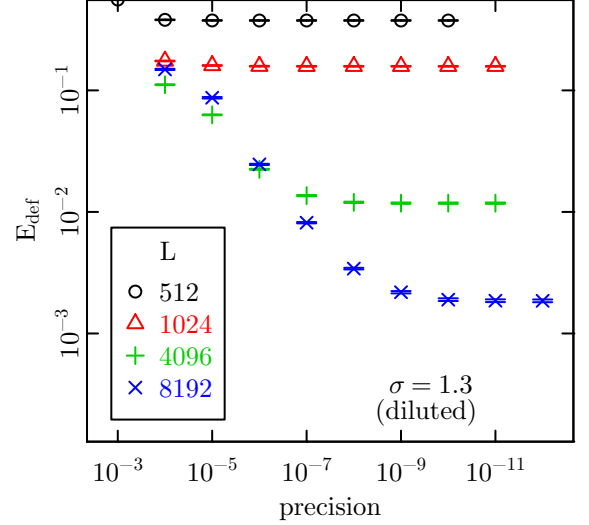


FIG. 10. (Color online). Convergence of the defect energy for the diluted model as a function of the precision of the ground-state energy calculation. For large  $\sigma$  this should be monitored accurately.

allow directly to measure the energy of a single defect seem preferable. For the case of the  $m = \infty$  spin glass on hypercubic lattices we indeed found different stiffness exponents from such “domain wall” BCs<sup>13</sup>. For the 1d long-range system, however, it is not obvious how to implement such alternative prescriptions.

The resulting energy differences are averaged,

$$E_{\text{def}} = [\Delta E]_{\text{av}} = [E_{AP} - E_P]_{\text{av}} \quad (67)$$

to yield an estimate  $E_{\text{def}}$  of the defect energy. Ground states were computed for  $\sigma$  in the interval  $0.1 \leq \sigma \leq 1$  for the diluted version of the model. For most of the values of  $\sigma$  a range of system sizes  $512 \leq L \leq 32768$  has been considered with about 3000 disorder realizations for larger and up to 10000 samples for smaller system sizes, see the parameters collected in Table I. We ensured convergence by monitoring  $E_{\text{def}}$  as the ground-state quench proceeds, cf. Fig. 10. This is of particular importance for large  $\sigma$ , where choosing a fixed precision fails to produce converged results for sufficiently large systems.

The averaged defect energies are shown for the available interaction ranges  $\sigma$  in Fig. 11. To extract the stiffness exponents, we performed fits of the functional form

$$E_{\text{def}} = aL^\theta(1 + b/L) \quad (68)$$

to the data. Similarly to our experience from the hypercubic systems, we found this form to describe the corrections rather well<sup>13</sup>. While this form parametrizes the leading analytical correction for  $\theta < 0$ , a constant would be asymptotically dominant over  $b/L$  for  $\theta > 0$ . Fits including a constant but no  $1/L$  correction, however, are not found to describe the data well for  $\theta > 0$ , such that

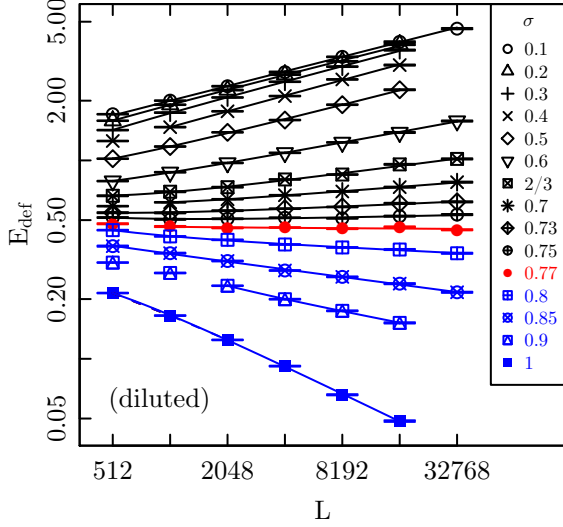


FIG. 11. (Color online). Defect energies for the diluted 1d power-law  $m = \infty$  spin glass as a function of lattice size  $L$  for a number of different interaction ranges  $\sigma$ . The solid lines show fits of the functional form (68) to the data. The corresponding fit parameters are summarized in Table I. The defect-energy exponent  $\theta$  changes sign in the vicinity of  $\sigma = 0.77$ , cf. Fig. 12.

we stick with the form (68) for all  $\sigma$ . Any non-analytic corrections, if present, appear to be sub-leading. These fits are shown in Fig. 11 and the corresponding fit parameters are collected in Table I. Fit qualities are found to be high throughout, indicating the suitability of the form chosen in Eq. (68).

Figure 12 summarizes our results for  $\theta$  as a function

TABLE I. Estimates of the spin stiffness exponent  $\theta$  in the *diluted* model resulting from fits of the functional form (68) to the data, including system sizes  $N_{\min} \leq N \leq N_{\max}$ .  $Q$  denotes the quality-of-fit.

$\sigma$	samples/ $10^3$	$aL^\theta(1+b/L)$		$\theta$	$Q$
		$N_{\min}$	$N_{\max}$		
0.1	2.4 – 10	32	32768	0.245(02)	0.12
0.2	2.9 – 10	512	16384	0.243(09)	0.39
0.3	3.1 – 9.1	512	16384	0.255(08)	0.70
0.4	3.3 – 9.5	1024	16384	0.260(12)	0.54
0.5	3.6 – 10	512	16384	0.245(08)	0.31
0.6	3.1 – 9.5	512	32768	0.177(06)	0.98
$2/3$	3.2 – 9.2	512	32768	0.126(07)	0.13
0.7	3.2 – 10	1024	32768	0.076(08)	0.96
0.73	3.2 – 9.1	512	32768	0.046(07)	0.89
0.75	3.2 – 9.1	512	32768	0.021(07)	0.56
0.77	3.2 – 9.3	1024	32768	−0.006(09)	0.28
0.8	3.2 – 9.0	512	32768	−0.046(06)	0.75
0.85	3.1 – 6.4	512	32768	−0.127(07)	0.44
0.9	2.8 – 10	2048	16384	−0.183(26)	0.65
1.0	1.8 – 9.7	512	16384	−0.467(09)	0.67

of  $\sigma$ . The stiffness exponent  $\theta$  clearly becomes constant at a value compatible with  $\theta = 1/4$  in the infinite-range regime  $\sigma \leq 1/2$ . To determine the upper critical  $\sigma_u$  where  $\theta(\sigma_u) = 0$ , we performed a linear fit to the results in the range  $0.5 \leq \sigma \leq 0.9$ , resulting in an intercept of  $\sigma_u = 0.76(3)$ . In connection with the observation of a linear behavior in the regime  $1/2 \leq \sigma \leq 3/4$ , this is compatible with the conjectured form  $\theta_{\text{LR}} = 3/4 - \sigma$ , cf. Eq. (49). This behavior is clearly different from the corresponding Ising spin-glass model with  $\theta_{\text{LR}} = 1 - \sigma$ . Notice that the change to the value  $1/4$  at  $\sigma = 1/2$  is not due to a failure of Eq. (49) for  $\sigma < 1/2$ , but because for  $\sigma < 1/2$  we have rescaled the bonds down by a factor of  $L^{1/2-\sigma}$ . If we had not done that  $\theta$  would have continued to be fitted by Eq. (49).

For larger  $\sigma$ , however, we observe clear deviations of the data for the diluted model from  $\theta = 3/4 - \sigma$ . In fact, the data for  $E_{\text{def}}$  at  $\sigma = 1.3$ , not shown in Fig. 11 (but see the lower left panel of Fig. 13), show a strong downward curvature, more resembling an exponential decay. A closer look reveals that there is no universality between the diluted and fully connected model for  $\sigma > 1$ , where the properties of the diluted graphs change significantly. As has been shown in Refs. 70 and 71, 1d graphs defined by Eq. (9) always percolate for  $\sigma \leq 1/2$  and they percolate for sufficiently large  $A$  (namely, for any  $z > 1/2$ ) in the regime  $1/2 < \sigma \leq 1$ . In contrast, percolation is (asymptotically) absent for  $\sigma > 1$ . For the defect-energy calculations considered here, this means that such non-percolating samples contribute  $\Delta E = 0$  to  $E_{\text{def}}$ , leading to much smaller averages than expected from the scaling Eq. (65). For the average coordination numbers considered here, such breakdown of percolation is only observed for very large systems, mostly beyond the reach of our numerical calculations. If we remove the links up to a finite range, however, for instance all nearest-neighbor links, the remaining graph does not percolate

TABLE II. Estimates of the spin stiffness exponent  $\theta$  in the *fully connected* model resulting from fits of the functional form (69) (for  $\sigma \leq 0.75$ ) and (68) (for  $\sigma > 0.75$ ), respectively, to the data.

$\sigma$	samples/ $10^3$	$N_{\min}$	$N_{\max}$	$\theta$	$Q$
0.1	3.9 – 4	64	4096	0.238(19)	0.98
0.2	3.9 – 4	64	4096	0.238(19)	0.06
0.3	3.9 – 4	64	4096	0.275(20)	0.12
0.4	3.9 – 4	64	4096	0.247(21)	0.31
0.5	3.9 – 4	64	4096	0.262(24)	0.76
0.57	3.9 – 4	128	4096	0.180(41)	0.86
0.6	3.8 – 4	128	4096	0.200(46)	0.52
0.625	3.9 – 4	64	4096	0.168(36)	0.52
0.75	3.8 – 4	64	4096	0.052(95)	0.87
0.8	3.8 – 4	256	4096	0.014(15)	0.73
1.0	2	256	4096	−0.209(21)	0.28
1.3	1.9 – 2	256	4096	−0.436(33)	0.99
2.0	1 – 2	256	2048	−1.132(37)	0.96
2.5	1 – 2	128	1024	−1.518(47)	0.96



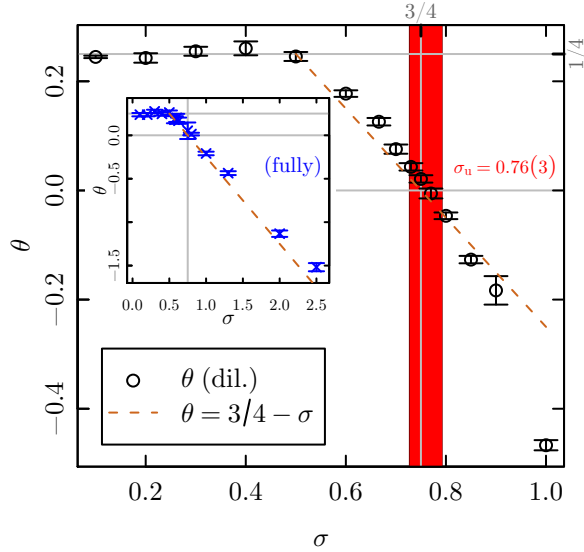


FIG. 12. (Color online). The stiffness exponent  $\theta$  extracted from the diluted model as a function of the interaction range exponent  $\sigma$ . See Table I for the corresponding fit parameters.  $\theta$  changes sign for the critical value  $\sigma_u = 0.76(3)$  marked by the shaded area. Below  $\sigma = 1/2$ , the spin stiffness exponent levels off at the infinite-range value  $\theta = 1/4$ . The dashed line denotes the conjectured form  $\theta = 3/4 - \sigma$ , cf. Eq. (49). The inset shows analogous results for the fully connected model and a wider range of  $\sigma$ .

for  $\sigma > 1$  already for moderate sizes such that the long-range nature is lost. An alternative way of understanding this phenomenon is to note that the diameters of the graphs considered here grow proportional to  $(\log L)^\delta$  for  $1/2 \leq \sigma < 1$ , corresponding to an infinite-dimensional or small-world graph, whereas they grow proportional to  $L$  for  $\sigma > 1$ , corresponding to a truly one-dimensional graph<sup>72</sup>. This explains the strong downwards deviations of  $\theta$  from the form  $\theta = 3/4 - \sigma$  seen in Fig. 12 for  $\sigma \geq 1$ . Right at  $\sigma = 1$ , we expect non-universality with  $\theta$  depending on the average coordination number  $z$  which, in turn, is a function of the parameter  $A$  in Eq. (9).

This is illustrated in Fig. 13 showing our estimates for  $\theta$  from diluted lattices with different average coordination numbers  $z$ . While, for  $\sigma < 1$ , the measured  $\theta$  is essentially independent of  $z$ , as expected, there is a dramatic  $z$  dependence right at  $\sigma = 1$ , with the non-universal  $\theta(z)$  approaching the value expected for the fully connected model in the limit  $z \rightarrow \infty$ . Similar  $z$  dependent critical behavior at  $\sigma = 1$  was also recently found for random walks on such graphs<sup>73</sup>. For  $\sigma > 1$ , on the other hand, the curves  $E_{\text{def}}$  cease to follow power laws and, instead, cross over to the  $\theta = -\infty$  or exponential decay expected for short-range one-dimensional systems<sup>9</sup>.

These deviations are specific to the diluted model: independent ground-state calculations for the fully connected model, summarized in the inset of Fig. 12, are consistent with  $\theta = 3/4 - \sigma$  also for  $\sigma > 1$ . The relevant

parameters and results for this model are summarized in Table II. In contrast to the diluted model, a constant was found to be a good description of the leading scaling corrections for  $\theta > 0$ , such that we used the form

$$E_{\text{def}} = aL^\theta + c \quad (69)$$

for  $\sigma \leq 3/4$  and the form (68) for  $\sigma > 3/4$ . Apart from the fact that only the fully connected model does represent the long-range universality class for  $\sigma \geq 1$ , we also find scaling corrections for  $\sigma < 1$  to be less pronounced there than for the diluted system, such that it appears questionable whether considering the diluted model offers a significant advantage in terms of the precision and accuracy of the final results.

Note that the results for  $\theta$  as  $\sigma$  is increased are in contrast to those for the Ising case, where  $\theta_{\text{SR}} = -1$ , so that the (fully connected) long-range Ising system is governed by short-range behavior for  $\theta_{\text{SR}} > \theta_{\text{LR}}$  viz.  $\sigma > 2$  (whereas the diluted Ising system would be truly short ranged already for  $\sigma > 1$ ). The  $m = \infty$  model, instead, is truly long-range everywhere, and crossover to the  $\theta_{\text{SR}} = -1$  of the nearest-neighbor 1d chain system is not seen. Instead, the limit  $\sigma \rightarrow \infty$  of our fully connected model corresponds to the 1d ladder system with<sup>9</sup>  $\theta = -\infty$ .

## V. FINITE-TEMPERATURE CALCULATIONS

The critical behavior which arises when  $\sigma < 3/4$  can only be studied with techniques appropriate to finite temperatures. While the ground-state calculations were greatly facilitated by the disappearance of metastability in the  $m \rightarrow \infty$  limit, the use of a saddle-point procedure permits the exact solution at finite temperatures. As will be discussed in this section, this approach leads to an iterative set of matrix equations that allow one to determine the thermally averaged spin-spin correlation function which, in turn, gives access to the Edwards-Anderson order parameter, the spin-glass susceptibility and the spin-glass correlation length. Due to the nature of the matrix equations, use of a diluted model does not have any computational advantages, so that all calculations have been performed on the fully connected model of Eq. (3).

### A. Saddle-point equations

The saddle-point equations for the  $m = \infty$  model were first derived in Ref. 10 and later discussed again in Refs. 6, 9, and 50. Starting point is the partition function corresponding to the Hamiltonian in Eq. (1),

$$Z = \int_{-\infty}^{\infty} \prod_{i,\mu} dS_i^\mu e^{\frac{\beta}{2} \sum_{i,j,\mu} J_{ij} S_i^\mu S_j^\mu} \prod_i \delta(m - \sum_\mu (S_i^\mu)^2). \quad (70)$$

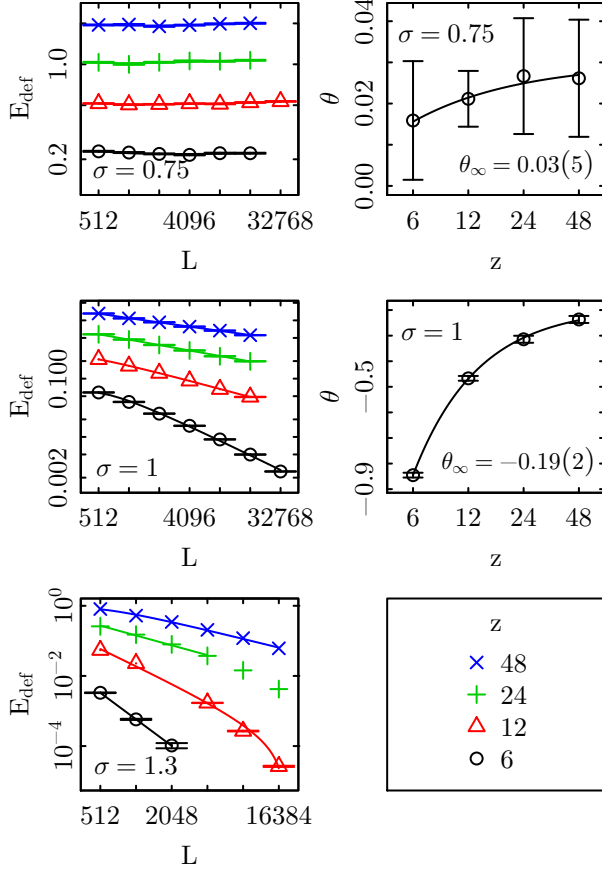


FIG. 13. (Color online). Dependence of defect energies and stiffness exponents in the diluted model on the average coordination number  $z$ . While for  $\sigma < 1$ , this is merely a finite-size correction, we observe a non-universal  $\theta$  for  $\sigma = 1$ , and non-power-law scaling implying an effective  $\theta = -\infty$  for  $\sigma > 1$ .

The spin integrations can be performed using integral representations of the  $\delta$  functions to yield

$$Z = \int_{-\infty}^{\infty} \prod_i \frac{\beta dH_i}{4\pi} \exp \left\{ \frac{m}{2} \left[ \sum_i \beta H_i + \ln \det \frac{\chi}{\beta} \right] \right\}, \quad (71)$$

where the susceptibility matrix  $\chi$  is defined by

$$\chi_{ij} = (A^{-1})_{ij} \quad (72)$$

$$A_{ij} = H_i \delta_{ij} - J_{ij}. \quad (73)$$

The  $H_i$  in Eq. (71) are initially just new integration variables introduced by the Fourier representation of the  $\delta$  constraints, but it will turn out that they have a profound physical meaning. The matrix  $A$  is obviously symmetric, since  $J_{ij} = J_{ji}$ . The correlation matrix,

$$C_{ij} = \frac{1}{m} \langle \mathbf{S}_i \cdot \mathbf{S}_j \rangle, \quad (74)$$

is identical to<sup>10</sup>

$$C_{ij} = T(A^{-1})_{ij}, \quad (75)$$

which can be seen via saddle-point approximation. Taking the normalization of the spins  $|\mathbf{S}_i| = \sqrt{m}$  into account and using Eq. (74), the main diagonal of  $C$  needs to be such that

$$C_{ii} = 1. \quad (76)$$

Then Eqs. (73), (75), and (76) can be solved self-consistently for the values of the  $N$  variables  $H_i$ . Eq. (76) is the saddle-point equation for the integrals in (71) and is valid as  $m \rightarrow \infty$  at fixed  $N$ .

At  $T = 0$  these equations are no longer well defined. Instead, as described above, it is a necessary condition for the system to be in a ground state for each spin to be aligned with its local molecular field  $\mathbf{H}_i$ , cf. Eq. (55). Due to the lack of metastability, for  $m \rightarrow \infty$  this condition is also sufficient. As was first noted in Ref. 50, for  $T \rightarrow 0$  the variables  $H_i$  of Eq. (73) are *equivalent* to the rescaled amplitudes  $|\mathbf{H}_i|/\sqrt{m}$  of the local fields.

It was suggested in Ref. 10 that the density  $\rho(\lambda)$  of (real) eigenvalues of  $\chi^{-1}$  or  $A$  was useful in discussions of the physics of random spin systems. For example, it was shown that the smallest eigenvalue would vanish at the critical temperature for  $N \rightarrow \infty$ . For the case of the  $m = \infty$  SK model in the thermodynamic limit,  $\rho(\lambda)$  follows a Wigner semicircle. Decreasing the temperature from  $T_{SG}$ , where the first eigenvalue vanishes, a fraction  $m_0 \sim N^{2/5}$  of eigenvalues becomes zero as  $T \rightarrow 0$ .<sup>6</sup> This corresponds to the contraction of the spin orientations into an  $m_0$ -dimensional subspace in the limit of zero temperature, an effect reminiscent of the Bose-Einstein condensation in atomic systems. The behavior of the eigenvalue density on cooling the system from high temperatures is illustrated for our 1d system in the infinite-range regime  $\sigma < 1/2$  in Fig. 14.

## B. Order parameter and spin-glass susceptibility

The saddle-point equations for systems on hypercubic lattices in two and three dimensions (as well as in the SK limit) have been previously examined by Lee, Dhar and Young in Ref. 15. They considered the correlation function  $C_{ij}$  of Eq. (75) and determined the Edwards-Anderson order parameter as

$$q_{EA}^2 = \lim_{r_{ij} \rightarrow \infty} [C_{ij}^2]_{av} \quad (77)$$

or as  $q_{EA}^2 = [C_{ij}^2]_{av}$ ,  $i \neq j$  for the SK model. Taking into account the scaling  $m_0 \sim N^\mu$  of the number of non-zero spin components, they concluded that  $q_{EA}^2 \sim N^{-\mu}$  in the ground state, i.e., that the order parameter vanishes in the thermodynamic limit. Similarly, defining

$$\chi_{SG}^0 = \frac{1}{N} \sum_{i,j} [C_{ij}^2]_{av} \quad (78)$$

they inferred algebraically decaying correlations  $[C_{ij}^2]_{av} \sim r_{ij}^{-d\mu}$  in the  $m = \infty$  model, i.e., merely quasi

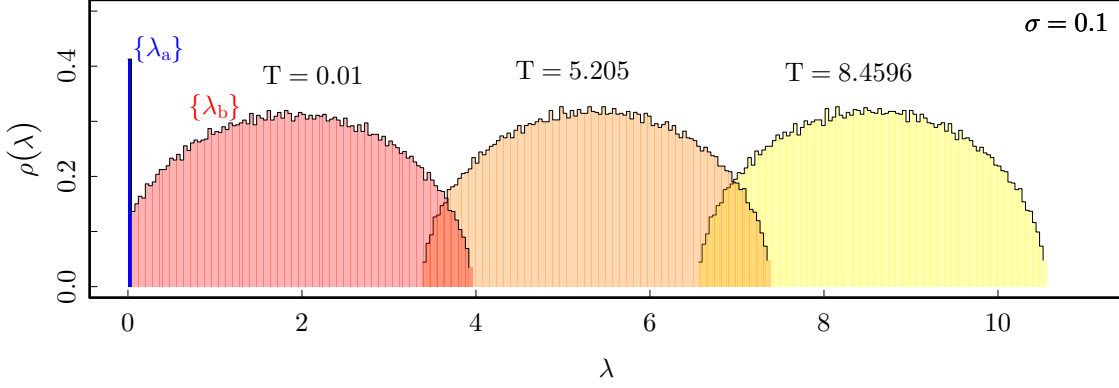


FIG. 14. (Color online). The eigenvalue density  $\rho(\lambda)$  of the matrix  $A$ , see Eq. (73), for the 1d  $m = \infty$  model at  $\sigma = 0.1$ . At high temperatures, the distribution follows Wigner's semicircle law<sup>6</sup>. Lowering the temperature shifts the whole distribution to the left, until for  $T \rightarrow 0$   $m_0$  eigenvalues  $\{\lambda_a\}$  vanish, while the majority  $(N - m_0)$  of eigenvalues  $\{\lambda_b\}$  stay finite. In the thermodynamic limit the Wigner semicircle law is restored again also there, since  $m_0/N \rightarrow 0$ .

long-range order. This is in contrast to the findings of Ref. 7 for the case of the  $N \rightarrow \infty$  limit being taken *before* the  $m \rightarrow \infty$  limit.

We believe, however, that one needs to consider the *connected* correlation function and *on-site* correlations to determine  $\chi_{SG}$  and  $q_{EA}$ , and we will see that this leads to different conclusions. The basic idea is to separate contributions from the zero and non-zero modes. Consider Eq. (74) and factor out the cumulant part  $\tilde{C}_{ij}$  of the correlation function,

$$C_{ij} = \frac{1}{m} \langle \mathbf{S}_i \rangle \cdot \langle \mathbf{S}_j \rangle + \underbrace{\frac{1}{m} (\langle \mathbf{S}_i \cdot \mathbf{S}_j \rangle - \langle \mathbf{S}_i \rangle \cdot \langle \mathbf{S}_j \rangle)}_{\tilde{C}_{ij}}. \quad (79)$$

Due to the symmetry of  $A$  and Eq. (75) the matrix  $C$  is also real and symmetric, and hence invertible. For the eigenvalues  $\lambda$  of  $A$  and  $\omega$  of  $C$ , we have the relation

$$\omega = \frac{T}{\lambda}. \quad (80)$$

Using the spectral theorem,  $C$  has an orthonormal basis of real independent eigenvectors  $\{\tilde{v}^n | n = 1, \dots, N\}$  for the set of eigenvalues  $\{\omega_n \in \mathbb{R}\}$ , which do not need to be distinct.

The spectral decomposition reads

$$C = \sum_{n=1}^N \omega_n \tilde{v}^n \cdot (\tilde{v}^n)^T, \quad (81)$$

where we use the outer product and the transpose denoted by  $(\cdot)^T$ . Thus, with  $(\tilde{v}^n)^T \cdot \tilde{v}^m = \delta_{mn}$  and for  $T < T_{SG}$ , the correlation matrix  $C$  has the eigenvalue decomposition

$$C_{ij} = \sum_{n=1}^N \omega_n v_i^n v_j^n = T \sum_a \frac{v_i^a v_j^a}{\lambda_a} + T \sum_b \frac{v_i^b v_j^b}{\lambda_b}, \quad (82)$$

where  $a = 1, \dots, m_0$  labels the  $m_0$  eigenvalues  $\lambda_a$  that vanish as  $T \rightarrow 0$ , and  $\lambda_b$ ,  $b = N - m_0 + 1, \dots, N$  refers to the remaining  $N - m_0$  eigenvalues which stay finite. Here,  $\lambda_x$  denotes the  $x^{\text{th}}$  eigenvalue and  $v_k^x$  is the  $k^{\text{th}}$  component of the corresponding normalized eigenvector  $\tilde{v}^x$  of  $A$ .

Working at  $m = m_0$  and using the reasonable assumption that the  $a^{\text{th}}$  component of the spin  $\mathbf{S}_i \in \mathbb{R}^{m_0}$  has the form

$$\langle S_i^a \rangle = \pm \sqrt{\frac{m_0 T}{\lambda_a}} v_i^a, \quad (83)$$

the cumulant part of the correlation function can be identified with

$$\tilde{C}_{ij} = T \sum_b \frac{v_i^b v_j^b}{\lambda_b}, \quad (84)$$

being a function of the non-vanishing eigenvalues. It is natural to define the spin-glass susceptibility in terms of this connected correlation function,

$$\begin{aligned} \chi_{SG} &= \frac{1}{Nm^2} \sum_{i,j} [\langle \mathbf{S}_i \cdot \mathbf{S}_j \rangle - \langle \mathbf{S}_i \rangle \cdot \langle \mathbf{S}_j \rangle]^2 \\ &= \frac{1}{N} \sum_{ij} \tilde{C}_{ij}^2 = \frac{T^2}{N} \sum_b \frac{1}{\lambda_b^2}, \end{aligned} \quad (85)$$

where the  $\lambda_b$  are the non-vanishing eigenvalues in the limit  $T \rightarrow 0$ . Furthermore, the Edwards-Anderson order parameter is then given by

$$\begin{aligned} q_{EA} &= \frac{1}{N} \sum_i \frac{\langle \mathbf{S}_i \rangle \cdot \langle \mathbf{S}_i \rangle}{m_0} = \frac{T}{N} \sum_i \sum_a \frac{v_i^a v_i^a}{\lambda_a} \\ &= \frac{T}{N} \sum_a \frac{1}{\lambda_a}, \end{aligned} \quad (86)$$



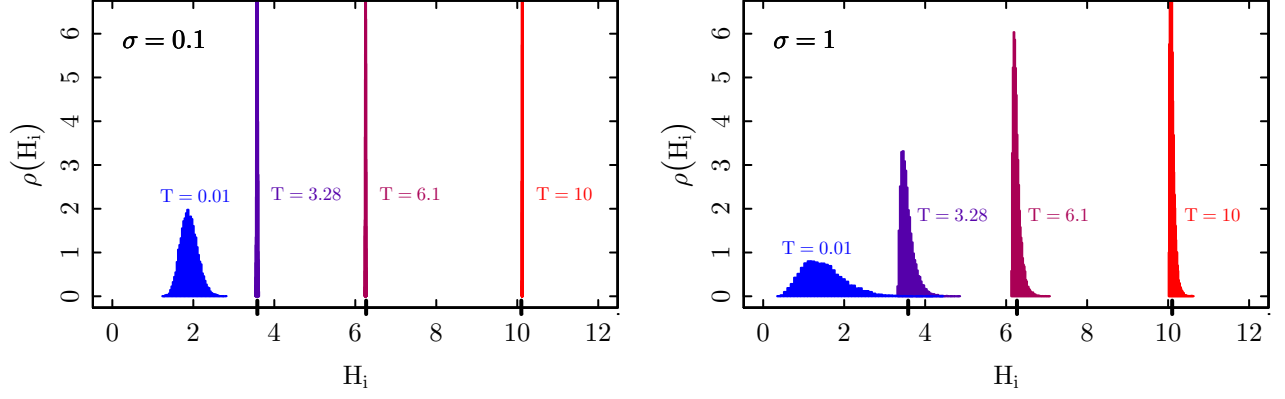


FIG. 15. (Color online). Density plots for the parameters  $H_i$  in Eq. (73) for  $\sigma = 0.1$  (left) and  $\sigma = 1.0$  (right). In the limit  $T \rightarrow 0$  they correspond to the (rescaled) local fields  $|\mathbf{H}_i|/\sqrt{m}$ . As is seen here, Eq. (94) yields suitable starting values for the iteration at high temperatures, cf. the bold ticks on the  $H_i$  axis. For increasing values of  $\sigma$  the distribution broadens. The normalization of the histograms is arbitrary. The system size used for this plot was  $N = 1448$ .

where the  $\lambda_a$  are the vanishing eigenvalues as  $T \rightarrow 0$ .

The chosen formalism leads to a non-vanishing order parameter at  $T = 0$ . To see this, consider

$$\frac{1}{N} \sum_{i=1}^N C_{ii} = \frac{T}{N} \sum_a \frac{1}{\lambda_a} + \frac{T}{N} \sum_b \frac{1}{\lambda_b} = 1 \quad (87)$$

resulting from the normalization condition  $C_{ii} = 1$ , Eq. (76). The finite eigenvalues  $\lambda_b$  scale to a constant as  $N \rightarrow \infty$  and  $T \rightarrow 0$ , hence the second sum in Eq. (87) is roughly proportional to  $N^{-1}N^{1-\mu} = N^{-\mu}$  and thus vanishes in the thermodynamic limit. Hence,  $q_{\text{EA}} = 1$  in this limit. The “zero” eigenvalues  $\lambda_a$  vanish as  $T \rightarrow 0$  and as  $N \rightarrow \infty$ . Assuming them to be proportional to  $T/N^p$ , we conclude from Eq. (87) that  $p = 1 - \mu$ .

### C. Numerical approach

We solve Eqs. (73), (75) and (76) iteratively using the Newton-Raphson method for systems with  $\sigma < 0.85$ , see the discussion in Ref. 15. For larger  $\sigma$ , this approach has some numerical instabilities leading to singular matrices in the course of the  $LU$  decomposition. We switched to a method using a  $QR$  decomposition similarly to the way Broyden’s method<sup>31</sup> is usually implemented. However, in both cases we utilized the exact Jacobian to speed up calculations. Next we will show that this extra speed-up comes for free. According to Eqs. (73), (75) and (76) we can proceed by introducing the  $N$  functions

$$f_i(\{H_k\}) = T(A^{-1})_{ii} - 1 \quad (88)$$

and solving for their zeroes. Taking into account  $A^{-1}A = \mathbf{1}$  we have

$$\frac{\partial \mathbf{1}}{\partial H_j} = \frac{\partial A^{-1}}{\partial H_j} A + A^{-1} \frac{\partial A}{\partial H_j} = \mathbf{0}, \quad (89)$$

so that after multiplying with  $A^{-1}$  from the right and solving for the needed derivative we arrive at

$$\frac{\partial A^{-1}}{\partial H_j} = -A^{-1} \frac{\partial A}{\partial H_j} A^{-1}. \quad (90)$$

By virtue of Eq. (73) it is

$$\left( \frac{\partial A}{\partial H_j} \right)_{nm} = \delta_{jn} \delta_{mn}, \quad (91)$$

such that we finally find

$$\begin{aligned} \left( \frac{\partial A^{-1}}{\partial H_j} \right)_{ii} &= - \sum_n \sum_m (A^{-1})_{in} \delta_{jn} \delta_{mn} (A^{-1})_{mi} \\ &= - (A^{-1})_{ij} (A^{-1})_{ji} = - (A^{-1})_{ij}^2. \end{aligned} \quad (92)$$

TABLE III. Realizations used for the  $T > 0$  calculations.

$\sigma$	samples/ $10^3$
0.1	0.9-2.4
0.2	0.7-1.5
0.3	0.9-2.0
0.4	0.9-2.0
0.5	0.9-1.4
0.51	0.8-1.3
0.54	0.7-2.3
0.57	0.7-2.4
0.6	1.0-3.2
$\frac{2}{3}$	0.9-1.3
0.7	0.8-1.4
0.73	1.0-2.9
0.75	1.0-1.9
0.77	1.0-2.8
0.8	0.9-2.8
0.85	0.9-2.8
0.9	0.7-2.0
1.0	0.2-2.0

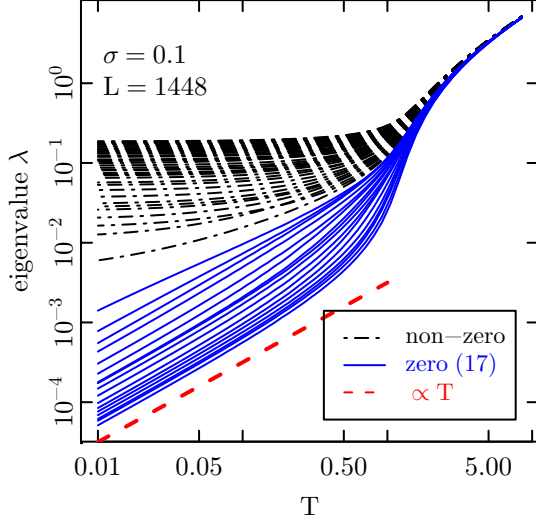


FIG. 16. (Color online). The evolution of eigenvalues  $\lambda$  of the matrix  $A$  of Eq. (73) with temperature for a  $L = 1448$  system with  $\sigma = 0.1$ . The non-zero eigenvalues (black, dot-dashed) stay finite in the limit  $T \rightarrow 0$  (biggest are left away). The others (blue, solid) scale to zero as  $\sim T$ . Note that both axes have logarithmic scales.

Hence the desired Jacobian reads

$$(J_f)_{ij} = \frac{\partial f_i}{\partial H_j} = -T (A^{-1})_{ij}^2. \quad (93)$$

We start the iterations at high temperature where we expect<sup>6</sup>

$$H_i = T + 1/T \quad (94)$$

for the SK model, resulting in reasonable initial values also for the 1d long-range system with  $\sigma > 0$  considered here. This is illustrated in Fig. 15 for  $\sigma = 0.1$  and  $\sigma = 1$ . For all systems considered here, we found a starting temperature of  $T_1 = 10$  to be a suitable and sufficient choice. The set of temperature points may be chosen in a geometrical fashion, such that the inverse temperature  $\beta = 1/T$  is distributed equidistantly. In all our simulations the lowest temperature was chosen to be  $T_f = 0.01$ . On decreasing the temperature, one may use the converged result of the previous calculation as a starting point. Alternatively, decreasing the temperature from  $T_k$  to  $T_{k+1}$  ( $k > 0$ ,  $T_{k+1} < T_k$ ) a new guess for the values of the  $H_i$  can be obtained by using the differential equation<sup>6</sup>

$$\frac{dH_i}{d\beta} = - \sum_j (B^{-1})_{ij}, \quad (95)$$

$$B_{ij} = (\beta C_{ij})^2. \quad (96)$$

To perform the analysis outlined above in Sec. VB, we need to separate zero from non-zero eigenvalues. For finite temperatures and finite systems, however, no eigenvalues are exactly zero. Instead, there is a difference

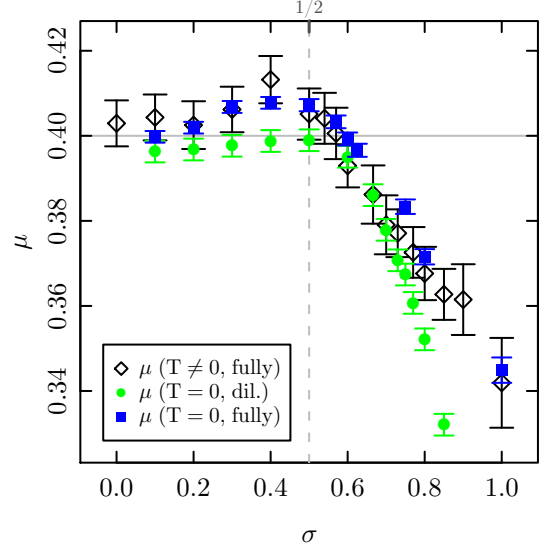


FIG. 17. (Color online). Spin-dimension exponent  $\mu$  calculated from the eigenvalue density at finite temperatures ( $T > 0$ ) as compared to the result reported in Sec. IV A from the ground-state computations ( $T = 0$ ). For  $\sigma = 0$  the SK model was considered directly. For the fully connected model, the results of the calculations at  $T = 0$  and for  $T > 0$  are well compatible.

in scaling behavior between the “zero” eigenvalues that vanish proportional to  $T/N^{1-\mu}$  and the other eigenvalues that scale to a constant. This is illustrated in Fig. 16. To automatically distinguish between the two types of eigenvalues, one might count all those as zero that fall below a chosen threshold at the lowest considered temperature. It turned out to be more reliable, however, to base the distinction criterion directly on the temperature scaling  $\propto T$  of the “zero” eigenvalues. Determining the slope of  $\log \lambda(T)$  at the lowest considered temperatures, we counted those eigenvalues as scaling to zero whose slope was above 0.5. Even with this rather reliable criterion, however, there will always be a certain ambiguity as the slopes change quite continuously over the different eigenvalues, and a number of borderline cases always exists, cf. the example in Fig. 16. We do not find any signs of the number of zero eigenvalues changing with temperature. Instead, our results are compatible with all relevant eigenvalues starting to scale to zero as soon as  $T < T_{SG}$ .

The analysis of the eigenvalue density allows for an alternative method of calculating the spin dimension scaling exponent  $\mu$  already discussed in Sec. IV A. To implement it, we determined the rank of the matrix  $M$  composed of the ground-state spin vectors. Instead, we could have extracted the local field values  $|\mathbf{H}_i|$ , fed them into Eq. (73) and determined the number of zero eigenvalues. These approaches are equivalent since the rows of  $M$  correspond to the null eigenvectors of  $A$  and the row and column ranks of a matrix are identical<sup>6</sup>. This

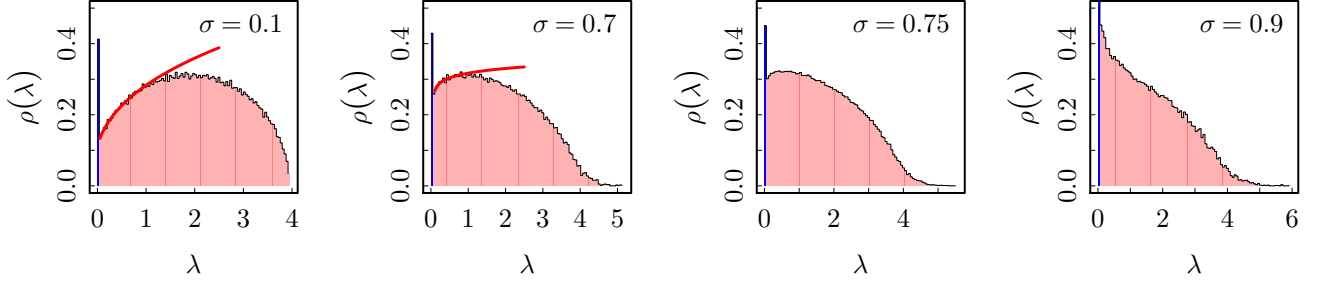


FIG. 18. (Color online). The eigenvalue distribution of the matrix  $A$ , cf. Eq. (73), at temperature  $T = 0.01$  for different values of the power-law exponent  $\sigma$  ( $N = 1448$ ). Wigner's semicircle form holds for the infinite-range region  $0 < \sigma \leq 1/2$  in the thermodynamic limit. The red, bold line shows fits of the functional form (99) to the data. A positive exponent  $x$  results for  $\sigma < 3/4$ .

would not have allowed us to consider sufficiently large systems, however, since there an  $N \times N$  matrix must be inverted, which is in contrast to the  $T = 0$  ground-state calculations where it was sufficient to determine the rank of the auxiliary, but smaller,  $m \times N$  ground-state spin matrix  $M$ . The results for  $m_0$  extracted from the finite-temperature calculation are summarized in Fig. 17. The outcomes are mostly compatible with those of the zero-temperature approach for the case of the fully connected model. In contrast, the  $T = 0$  results for the diluted model systematically deviate from those of the fully connected model for  $\sigma > 1$  as discussed above in Sec. IV B, and some signs of this non-universality are already seen for  $\sigma \gtrsim 0.8$ .

#### D. Distribution of eigenvalues

Braun and Aspelmeier<sup>58</sup> suggested using the eigenvalue spectrum for a more general understanding of scaling corrections for the case of the two competing limits  $N \rightarrow \infty$  and  $m \rightarrow \infty$ . Their analysis is valid for the system on a Bethe lattice, but some results might generalize to the model considered here. They discuss the ground-state energy  $e(m, N) = E/Nm$  per spin and spin component, which is argued to have two contributions: the ground-state energy in the limit  $N \rightarrow \infty$  with  $m = m_0$  large and fixed,  $e_\infty + \frac{1}{4}m_0^{-y} + O(m_0^2)$ , and the additional energy required for forcing the  $N$  spins into an  $m_0$  dimensional subspace. This second contribution is proportional to the required shift of the eigenvalue spectrum  $\rho(\lambda)$  to push  $m_0$  eigenvalues to zero. Assuming the density at small  $\lambda$  to scale as  $\rho(\lambda) \sim \lambda^x$ ,<sup>10</sup> the first  $m_0$  eigenvalues occupy the interval  $[0, (m_0/N)^{1/(1+x)}]$ , such that the total energy is

$$e(m, N) = e_\infty + c_1 m_0^{-y} + c_2 \left( \frac{m_0}{N} \right)^{1/(1+x)}. \quad (97)$$

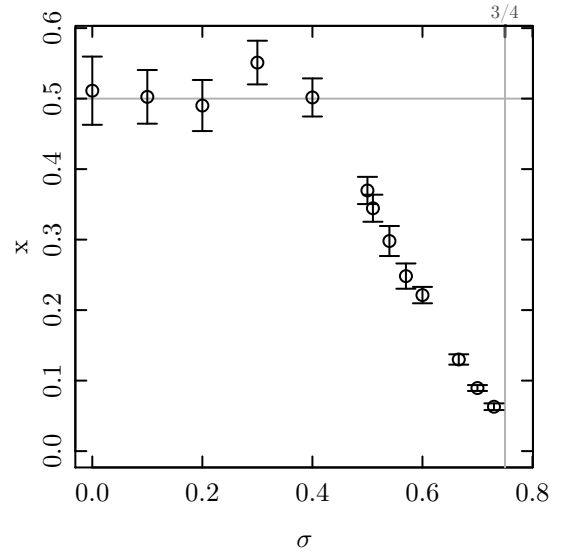


FIG. 19. (Color online). The density exponent  $x$  as determined by fitting a power-law, Eq. (99), to the eigenvalue densities shown in Fig. 18.

Minimizing with respect to the number  $m_0$  of spin components yields the scaling relation

$$\mu = \frac{1}{y(x+1)+1}. \quad (98)$$

For the SK model with  $x = 1/2$  (the Wigner semicircle law) and  $y = 1$ ,<sup>8</sup> we therefore arrive at the observed  $\mu = 2/5$  as desired. This scaling should hold independent of lattice structure.

We determined the exponent  $x$  of the density of eigenvalues as  $\lambda \rightarrow 0$  from fits of the functional form

$$\rho(\lambda) = a(\lambda + \Delta\lambda)^x \quad (99)$$

to the data. Here, the shift  $\Delta\lambda$  is required to take the zero eigenvalues into account. To perform the fits, eigenvalues

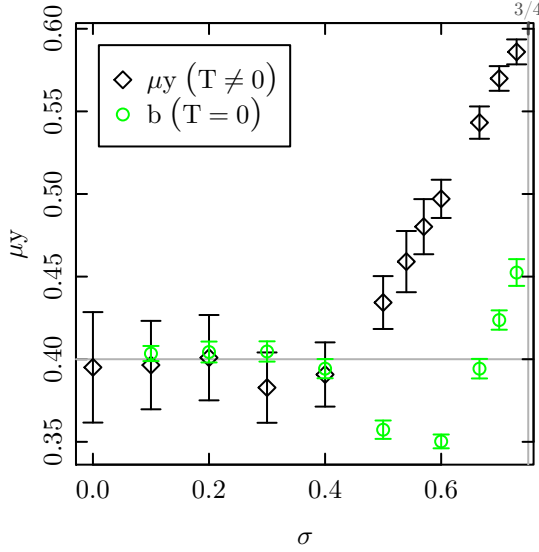


FIG. 20. (Color online). A comparison of the exponent  $z = (1 + \mu)/(1 + x)$  determined from the  $T > 0$  calculations (black diamonds) with the ground-state energy correction exponent  $b$  as determined in Sec. IV A (green circles).

from a large number of disorder samples were accumulated, and the limit  $\lambda \rightarrow 0$  was modeled by successively omitting more of the larger eigenvalues while monitoring the resulting estimate of  $x$  as well as the goodness-of-fit. Statistical errors on the fit results were determined using a sophisticated jackknifing analysis<sup>74</sup>. Some example results are collected in Fig. 18. Fits of this functional form are possible for  $\sigma < 3/4$ , where the vanishing of the phase transition is signaled by  $x = 0$ . This is expected since at the upper critical value  $\sigma_u = 3/4$  the vanishing of eigenvalues at any finite temperature ceases to exist<sup>10</sup>. Collecting the results for all values of  $\sigma$  considered, we arrive at the data shown in Fig. 19 which confirms our expectations of  $x = 1/2$  for  $\sigma \leq 1/2$  and  $x = 0$  for  $\sigma = 3/4$ . In view of the above expectations which are in-line with our numerical results, it is tempting to speculate that  $x(\sigma) = 3/2 - 2\sigma$ , but we have not been able to substantiate this claim with a theoretical argument.

Additionally, the authors of Ref. 58 suggest the scaling ansatz

$$e(m, N) - e_\infty = m^{-y} F(mN^{-\mu}) \quad (100)$$

where  $F(x)$  is a scaling function. In the relevant limit of  $m \rightarrow \infty$  before  $N \rightarrow \infty$ , this implies a scaling of the ground-state energy according to

$$e(m = \infty, N) - e_\infty \sim N^{-z} \quad (101)$$

with  $z = \mu y = (1 - \mu)/(1 + x)$ , where we used Eq. (98). In Fig. 20 we show the correction-to-scaling exponent  $b$  for the ground-state energies as determined in Sec. IV A in comparison to  $z = (1 - \mu)/(1 + x)$  as determined from the results of  $\mu$  and  $x$  for our system. Both exponents

agree for  $\sigma \leq 1/2$  where  $b = z = 2/5$ . For larger values of  $\sigma$ , however,  $b$  is consistently smaller than  $z$ . Therefore, if the corrections predicted here are present, they are sub-leading and cannot be resolved by our numerical analysis.

## E. Critical behavior

We now turn to studying the behavior of the physical observables extracted from the solution to the saddle-point equations in the vicinity of the critical point. The analysis of the spin-glass correlation length, the Edwards-Anderson order parameter and the spin-glass susceptibility allows us to compare our simulations to the theoretical predictions outlined in Sec. III D.

### 1. Correlation length

The spin-glass correlation function can be calculated from the spin-spin correlation function (75) via

$$G_{\text{SG}}(r) = \frac{1}{L} \sum_{r_{ij}=r} [C_{ij}^2]_{\text{av}} = \frac{T^2}{L} \sum_{r_{ij}=r} [(A^{-1})_{ij}^2]_{\text{av}}. \quad (102)$$

Note that here we use the algebraic graph distance  $r_{ij}^1 = \min(|i - j|, L - |i - j|)$  irrespective of whether the ring or chain geometry is considered. To arrive at the usual second-moment definition of the correlation length, we use the Fourier decomposition,

$$\begin{aligned} \chi_{\text{SG}}^0(k) &= \frac{T^2}{L} \sum_{i,j} [(A^{-1})_{ij}^2]_{\text{av}} e^{ik[(i-j) \bmod L]} \\ &= \frac{T^2}{L} \sum_{i,j} [(A^{-1})_{ij}^2]_{\text{av}} \cos(k[(i-j) \bmod L]) \\ &= 2 \sum_{r=0}^{\lfloor L/2 \rfloor} G_{\text{SG}}(r) \cos(kr), \end{aligned} \quad (103)$$

and plug it into Eq. (32),

$$\xi_L = \frac{1}{2 \sin(k_{\min}/2)} \left[ \frac{\chi_{\text{SG}}^0(0)}{\chi_{\text{SG}}^0(k_{\min})} - 1 \right]^{1/(2\sigma-1)}. \quad (104)$$

Here,  $k_{\min} = 2\pi/L$ . In practice, we determine  $G_{\text{SG}}(r)$  per disorder realization from the saddle-point equations. For space efficiency, storing  $G_{\text{SG}}(r)$  is then preferable over storing  $C_{ij}$  directly. Note that since we are using the disconnected correlation function here, the estimators (104) only represent the correlation length above  $T_{\text{SG}}$ . Close to criticality, we expect the scaling form

$$\xi_L \sim \begin{cases} L^{\nu/4} \mathcal{X}(tL^{1/4}), & 1/2 < \sigma \leq 5/8, \\ L \mathcal{X}(tL^{1/\nu}), & \sigma > 5/8. \end{cases} \quad (105)$$

In the ordered phase, on the other hand,  $\xi_L$  diverges even more strongly with the system size<sup>75</sup>. As a consequence,

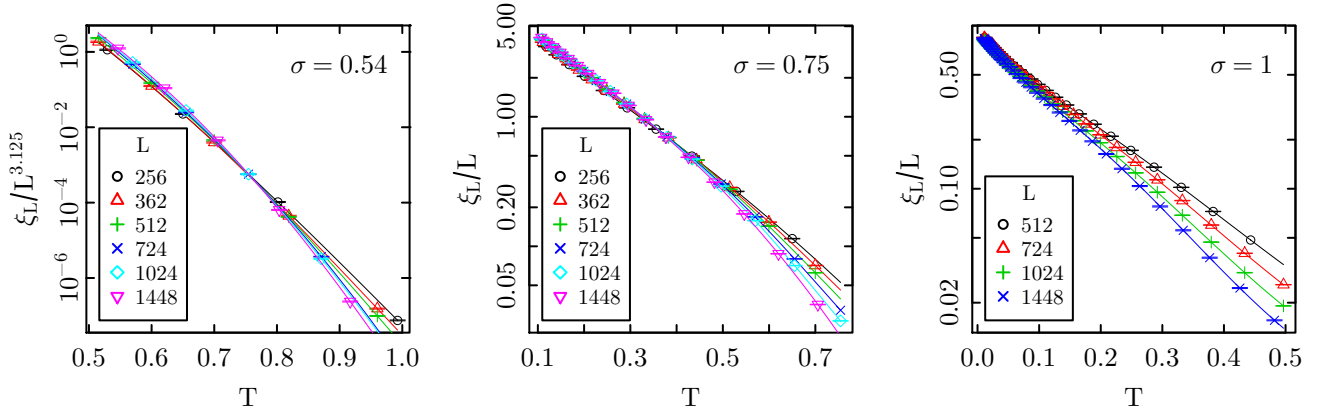


FIG. 21. (Color online). The spin-glass correlation length  $\xi_L/L$  (for  $\sigma \geq 5/8$ ) and  $\xi_L/L^{\nu/4}$  (for  $1/2 < \sigma < 5/8$ ), respectively, for different lattice sizes  $L$ . For  $\sigma < 3/4$  lines show a clear crossing point. The crossing vanishes at  $\sigma = 3/4$ , where the lines for lattice sizes  $L = N > 362$  lie approximately on top of each other below a certain temperature.

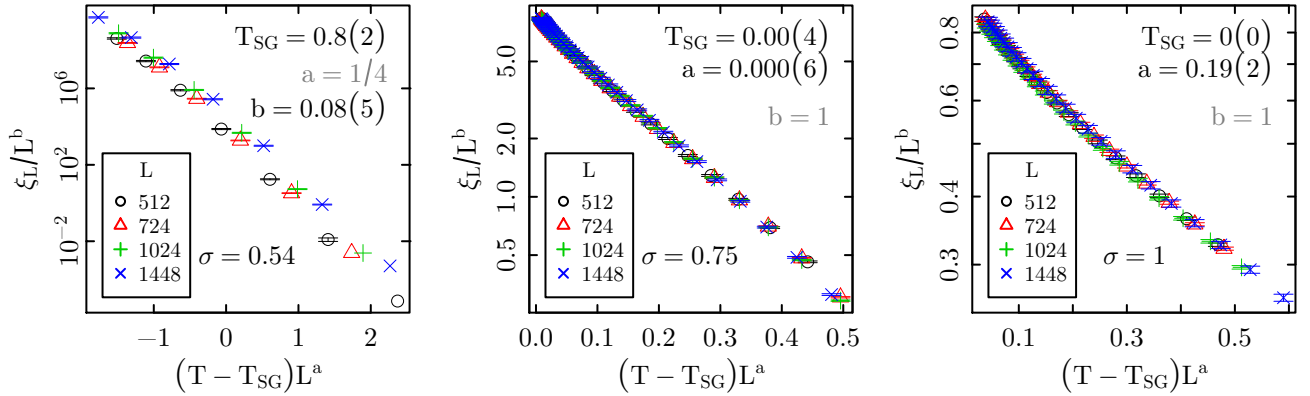


FIG. 22. (Color online). Scaling collapse of the correlation length ratios  $\xi_L/L$  and  $\xi_L/L^{\nu/4}$ , respectively. For optimizing parameters, a general form  $\xi_L = L^b \mathcal{X}(tL^a)$  was assumed. For  $\sigma > 3/4$  the transition temperature was fixed at  $T_{SG} = 0$ , since the according collapses yielded values around zero. The resulting parameters are summarized in Fig. 23.

the curves for  $\xi_L/L$  ( $\sigma \geq 5/8$ ) and  $\xi_L/L^{\nu/4}$  ( $1/2 < \sigma < 5/8$ ), respectively, will cross in the vicinity of the critical temperature.

Plots of  $\xi_L/L$  and  $\xi_L/L^{\nu/4}$  resulting from the finite-temperature calculations with parameters summarized in Tab. III for three examples of  $\sigma$  are shown in Fig. 21. Below  $\sigma_u = 3/4$ , we find a crossing of the curves as shown for  $\sigma = 0.54$ . For  $\sigma > 3/4$ , on the other hand, the curves only merge in the limit  $T \rightarrow 0$ . At the critical  $\sigma$ , we see a merging of the curves with an onset temperature scaling to 0 as  $L \rightarrow \infty$ . We note that the scaling of  $\xi_L/L^{\nu/4}$  is hard to observe numerically for  $\sigma$  close to  $1/2$ , where  $\nu = 1/(2\sigma - 1) \rightarrow \infty$ , such that a crossing point of  $\xi_L/L^{\nu/4}$  is not visible for the system sizes considered here for  $\sigma = 0.51$ . It is possible to extract estimates for the spin-glass temperature  $T_{SG}$  and the correlation length exponent  $\nu$  by re-scaling the data for different system sizes such that they collapse on the scaling function  $\mathcal{X}(x)$ . We used two complementary approaches for per-

forming this collapse: method (a) consists of a joint fit of all data sets to a third-order polynomial approximating the scaling function in the chosen regime; method (b) is the collapsing procedure suggested in Ref. 76 which, in turn, is based on Ref. 77. In both cases, we performed the collapse on the *logarithm* of the actual data. This turns out to be necessary since, in particular for small  $\sigma$ ,  $\xi_L/L$  spans many orders of magnitude in the range of temperatures considered here. In some cases, we also employed weights of the data points involved that decay exponentially away from the adaptively chosen value of the critical temperature. Statistical errors on the collapse parameters have been determined by a bootstrap sampling over the whole collapsing procedure<sup>74</sup>. In the region  $\sigma > 5/8$ ,  $\nu$  was determined from the scale  $tL^{1/\nu}$  of the abscissa. On the contrary, for the mean-field region  $1/2 < \sigma \leq 5/8$ , it was determined from the scaling  $\xi_L/L^{\nu/4}$  of the ordinate. For the latter collapses, we find that the expected scaling of  $tL^{1/4}$  of the argument of the

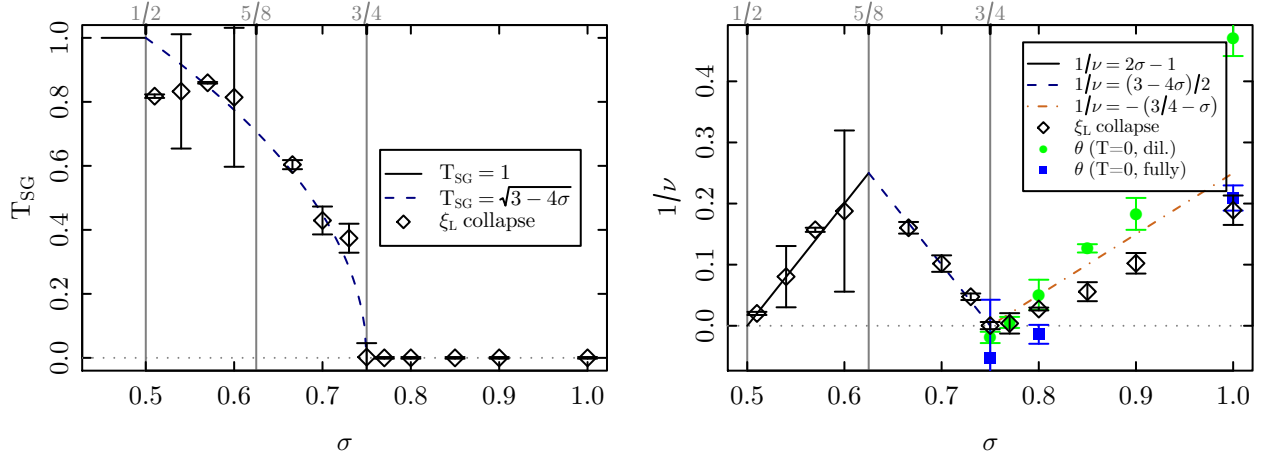


FIG. 23. (Color online). Spin-glass transition temperature  $T_{SG}$  and correlation length exponent  $\nu$  as estimated from collapses of the correlation length data according to the functional form Eq. (105). Left panel: transition temperature  $T_{SG}$  as compared to the prediction  $T_{SG} = \sqrt{3 - 4\sigma}$  of Eq. (51). Right panel:  $1/\nu$  and the relations  $1/\nu = 2\sigma - 1$  valid in the mean-field region  $1/2 < \sigma \leq 5/8$ , cf. Eq. (34), and  $1/\nu \approx (3 - 4\sigma)/2$ , cf. Eq. (52). For  $\sigma > 3/4$ , where  $T_{SG} = 0$ , we additionally show  $1/\nu = -\theta$  with our estimates of  $\theta$  resulting from the defect-energy calculations, as well as the conjectured  $1/\nu = -\theta = \sigma - 3/4$ .

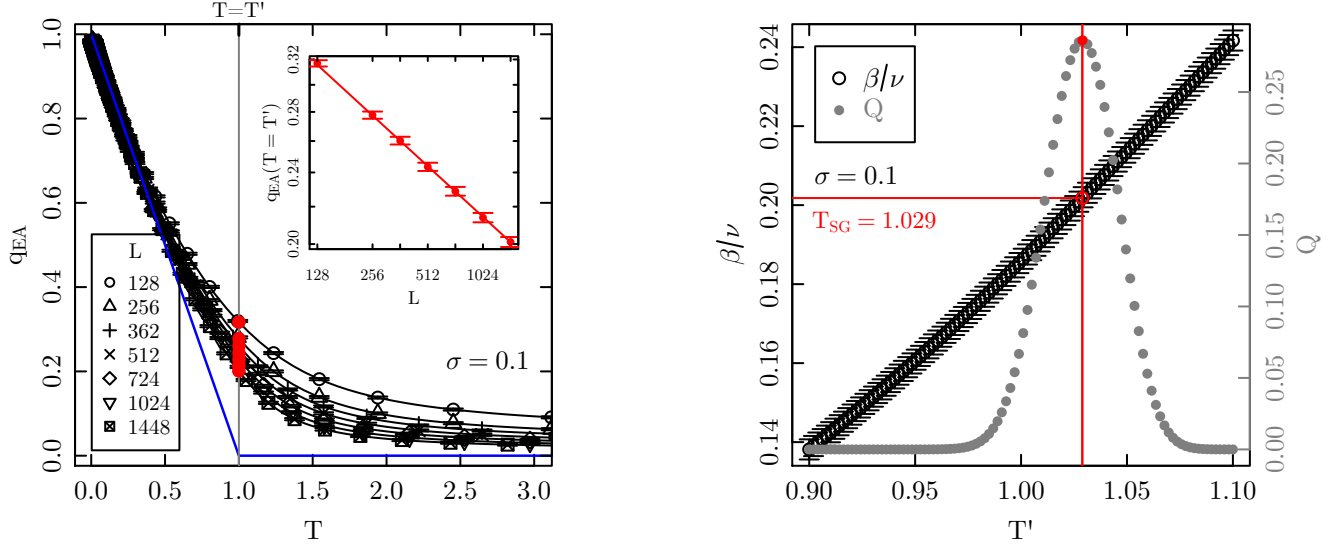


FIG. 24. (Color online). Scaling of the Edwards-Anderson order parameter  $q_{EA}$ . The left panel shows the dependence of  $q_{EA}$  on temperature for  $\sigma = 0.1$ . For  $L \rightarrow \infty$ , we expect the form (107) which is indicated by the solid blue line. Employing fits of the functional form (108) for a temperature interval  $T_i \leq T' \leq T_f$  around the expected critical temperature (see inset of left panel), we determine  $T_{SG}$  and  $\beta/\nu$  from the point where such fits work best, which is monitored by the quality-of-fit parameter  $Q$ , shown in the right panel. For a summary of results for all  $\sigma$  see Fig. 25.

scaling function is not very well reproduced, and we allow for this exponent to fluctuate to accommodate scaling corrections.

As illustrated in Fig. 22, these collapses work rather well over the whole range of  $\sigma$ . The resulting estimates of the correlation length exponent  $\nu$  and the critical temperature are summarized in Fig. 23. The transition temperature is consistent with  $T_{SG} = 0$  for  $\sigma \geq 3/4$  and approaches  $T_{SG} = 1$  as  $\sigma \rightarrow 1/2$ . In between, it is com-

patible with the estimate  $T_{SG} \approx \sqrt{3 - 4\sigma}$  obtained in Sec. III D. As mentioned above, in the mean-field regime with  $\sigma \rightarrow 1/2+$ , finite-size corrections become very pronounced due to the divergent exponent  $\nu$ . This leads to rather strong fluctuations of  $\nu$  and  $T_{SG}$  as estimated from the collapsing procedures, cf. Fig. 23. In the right panel of this figure we also compare our result for  $1/\nu$  extracted from collapses for  $\sigma > 3/4$  with  $-\theta$  from the defect-energy calculations. In general, we find acceptable



agreement between zero- and finite-temperature calculations. The observed systematic deviations give an indication of the level of unresolved finite-size corrections. As  $\sigma \rightarrow 1-$ , results for the diluted system start to systematically deviate from those for the fully connected system due to the observed non-universality discussed in Sec. IV B.

Comparing the estimates for  $1/\nu$  and  $T_{\text{SG}}$  for the ring, line and resummed line geometries introduced in Sec. II B, we find complete consistency, cf. the example results for  $\sigma = 3/4$  collected in Table IV.

### 2. Edwards-Anderson order parameter

According to the discussion of FSS in our model, we expect

$$q_{\text{EA}} \sim \begin{cases} L^{-1/4} Q(tL^{1/4}), & \sigma \leq 5/8, \\ L^{-\beta/\nu} Q(tL^{1/\nu}), & \sigma > 5/8. \end{cases} \quad (106)$$

for temperatures in the scaling window. In the thermodynamic limit, for  $\sigma < 1/2$ ,  $\beta = 1$ ,<sup>6,7</sup> while for  $\sigma > 5/8$ ,  $\beta$  is expected to remain close to unity, so that

$$q_{\text{EA}} \approx \begin{cases} 1 - T/T_{\text{SG}}, & T < T_{\text{SG}}, \\ 0, & T \geq T_{\text{SG}}. \end{cases} \quad (107)$$

As is illustrated with the unscaled data in the left panel of Fig. 24, these expectations are borne out well by our results. In particular, the thus defined order parameter becomes unity as  $T \rightarrow 0$ , in contrast to the differently defined  $q_{\text{EA}}^0$  of Eq. (77) and Ref. 15.

Right at  $T_{\text{SG}}$ ,  $q_{\text{EA}}$  scales to zero. To extract  $T_{\text{SG}}$  and determine  $\beta/\nu$ , we again employed scaling collapses. Due to the observed instability of the collapsing procedure, we also developed an independent approach based on the quality of power-law scaling. Since scaling proportional to  $L^{\beta/\nu}$  is only expected at criticality, the critical point might be determined under the assumption that it coincides with the temperature where power-law scaling is best observed. We hence performed fits according to the form

$$q_{\text{EA}}(T = T') = cL^{\beta/\nu}, \quad (108)$$

for an interval of temperatures  $T_i \leq T' \leq T_f$  around the expected value of  $T_{\text{SG}}$ . If power-law scaling only occurs at  $T = T_{\text{SG}}$  asymptotically, the quality-of-fit parameter  $Q$  should be maximized at this point, such that the information of both the critical temperature and the exponent  $\beta/\nu$  can be extracted by this procedure. An example for this approach for  $\sigma = 0.1$  is shown in the right panel of Fig. 24.

The overall results for the transition temperature  $T_{\text{SG}}$  and the critical exponent  $\beta/\nu$  resulting from this analysis are summarized in Fig. 25, together with the corresponding results of a collapsing procedure. The estimates of the spin-glass temperature are consistent with

$T_{\text{SG}} = \sqrt{3 - 4\sigma}$  in the relevant regime and become constant at  $T_{\text{SG}} = 1$  for  $\sigma \leq 1/2$ , while they vanish for  $\sigma > 3/4$ , as expected. From the present analysis,  $T_{\text{SG}}$  can be resolved with more precision than from the correlation length particularly in the mean-field regime  $\sigma < 5/8$ . The exponent  $\beta/\nu$  is consistent with the expectations summarized in Sec. III D, i.e.,  $\beta/\nu = 1/4$  for  $\sigma < 5/8$  and  $\beta/\nu = (3 - 4\sigma)/2$  for  $5/8 < \sigma \leq 3/4$ . The statistical precision of our determination, however, is not sufficient to rule out possible different scenarios and, in particular, to decide whether  $\beta/\nu = (3 - 4\sigma)/2$  might be exact in the non-mean-field regime. Again, statistical errors are calculated by an elaborate jackknifing procedure. As shown in Table IV, no significant deviations between the results for the different models of a 1d geometry are observed.

### 3. Spin-glass susceptibility

We finally analyzed the scaling behavior of the spin-glass susceptibility as defined from the connected correlation function in Eq. (85). From the discussion in Sec. III D we expect scaling according to

$$\chi_{\text{SG}} \sim \begin{cases} L^{1/4} \mathcal{C}(tL^{1/4}) & \sigma \leq 5/8, \\ L^{\gamma/\nu} \mathcal{C}(tL^{1/\nu}) & \sigma > 5/8. \end{cases} \quad (109)$$

In contrast to the scaling of  $q_{\text{EA}}$  it is possible here without reference to numerical derivatives to define a series of pseudo-critical temperatures from the locations of the maxima of the susceptibility,

$$T_{\text{SG}}^{(\text{max})} = T_{\text{SG}} + cL^{-1/\nu}, \quad (110)$$

while the values of  $\chi_{\text{SG}}$  at the maxima should then follow

$$\chi_{\text{SG}}^{(\text{max})} = cL^{\gamma/\nu}. \quad (111)$$

Fits of the corresponding forms to the data for  $\sigma = 0.1$  are shown in Fig. 26. We find, however, that the resulting parameter estimates are afflicted by very strong finite-size corrections. In particular, the resulting estimates of  $1/\nu$  are far off from our theoretical predictions as well as the results from the analysis of the correlation length.

The presence of strong corrections in the scaling of  $\chi_{\text{SG}}$  is well-known from studies, e.g., of the Ising spin glass. It

TABLE IV. Results for different choices of the geometry of the model, which were introduced in Sec. II B. There are no significant differences for the value  $\sigma = 3/4$  checked here.

quantity	ring	line	summed line
$\mu$	0.372(6)	0.374(8)	0.371(7)
$\xi_L$			
$1/\nu$	0.000(5)	-0.01(1)	-0.03(5)
$T_{\text{SG}}$	0.00(4)	0.04(6)	0.01(16)
$q_{\text{EA}}$			
$\beta/\nu$	0.01(4)	-0.02(5)	0.00(2)
$T_{\text{SG}}$	0.06(19)	-0.09(27)	0.00(13)

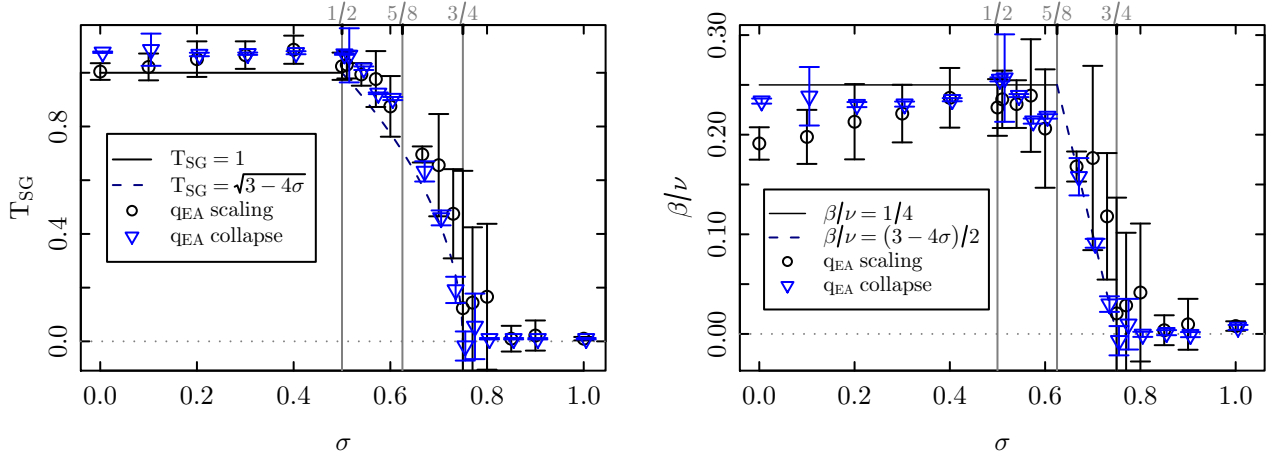


FIG. 25. (Color online). Transition temperature  $T_{\text{SG}}$  and critical exponent  $\beta/\nu$  as extracted from the  $Q$ -maximization procedure described in the main text and in Fig. 24. As a comparison we extracted these quantities from a data collapse as well.

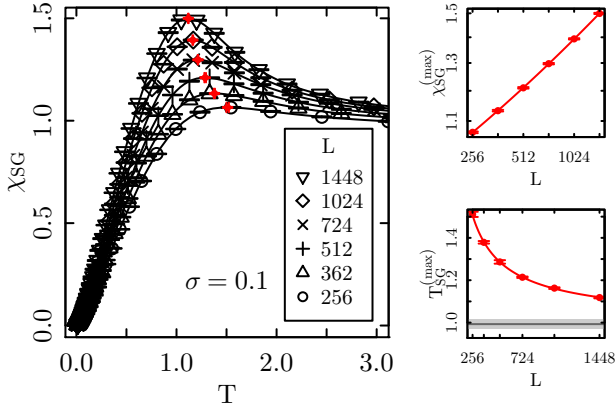


FIG. 26. (Color online). Scaling of maxima of the spin-glass susceptibility  $\chi_{\text{SG}}$  in a showcase example with  $\sigma = 0.1$ .

has been suggested<sup>78</sup> that modified scaling forms incorporating scaling corrections might contribute towards resolving such corrections and the proposed extended scaling forms have been successfully applied to the Ising spin glass<sup>79</sup>. In particular, one problem of the scaling form (109) is that it cannot reproduce the observed behavior  $\chi_{\text{SG}} \rightarrow 1$  as  $T \rightarrow \infty$ , cf. Fig. 26: assuming that  $\mathcal{C}(x) \sim x^\alpha$  for  $x \gg 1$ , asymptotic size independence of the data at large  $T$  requires that  $\alpha = -\gamma$  and hence  $L^{\gamma/\nu} \mathcal{C}(tL^{1/\nu}) \rightarrow 0$  as  $T \rightarrow \infty$ . While this is not in contradiction to scaling theory as the assumed scaling form should only apply in the critical region, having a scaling form consistent with the behavior as  $T \rightarrow 0$  or  $T \rightarrow \infty$  might allow to extend the scaling regime or, equivalently, reduce the observed finite-size corrections. A modified scaling form that serves this purpose is given by<sup>78</sup>

$$\chi_{\text{SG}} = (LT)^{\gamma/\nu} \tilde{\mathcal{C}}[(LT)^{1/\nu} t], \quad (112)$$

which is compatible with  $\chi_{\text{SG}} \rightarrow 1$  as  $T \rightarrow \infty$ . We

used this extended scaling form to perform collapses of the finite-size data for the spin-glass susceptibility. Even though some scaling corrections are implicitly included in Eq. (112), these collapses are found to be rather unstable and, hence, sensitive to the choice of starting values for the parameters and the range of data points to be included for each lattice size. In view of these uncertainties, we found it impossible to extract all three parameters,  $T_{\text{SG}}$ ,  $\gamma/\nu$  and  $1/\nu$  reliably from a single collapsing procedure. We hence decided to keep  $T_{\text{SG}}$  fixed at the theoretical prediction  $T_{\text{SG}} = \sqrt{3-4\sigma}$  which, as is shown in the results of Fig. 24 for the order parameter, is well compatible with our numerical results. An example collapse is shown in the left panel of Fig. 27. The right panel shows our resulting estimates of  $\gamma/\nu$  for  $\sigma \leq 0.8$ . These are roughly compatible with our expectations of  $\gamma/\nu = 0.25$  for  $\sigma \leq 5/8$  and  $\sigma/\nu = 2\sigma - 1$  for  $\sigma > 5/8$ . For  $\sigma \gtrsim 3/4$ , we do not find stable collapses with reasonable parameters which we attribute to the fact that, there,  $T_{\text{SG}} = 0$ , but our data only reach down to  $T_{\text{min}} = 0.01$ . The resulting values of  $1/\nu$  are strongly fluctuating and hence not useful as reliable estimates of this quantity. An alternative collapsing exercise using a plot of  $\chi_{\text{SG}}$  as a function of  $\xi/L$ , which should have the theoretical advantage of involving only a single adjustable parameter  $\gamma/\nu$  did, unfortunately, not lead to more reliable results.

## VI. CONCLUSIONS

We have used extensive numerical simulations together with a number of phenomenological scaling arguments to give a rather comprehensive account of the critical behavior of the one-dimensional spin-glass model with power-law interactions in the limit of an infinite number of spin components  $m$ . Compared to the more familiar case with  $m < \infty$ , we find a number of remarkable differ-



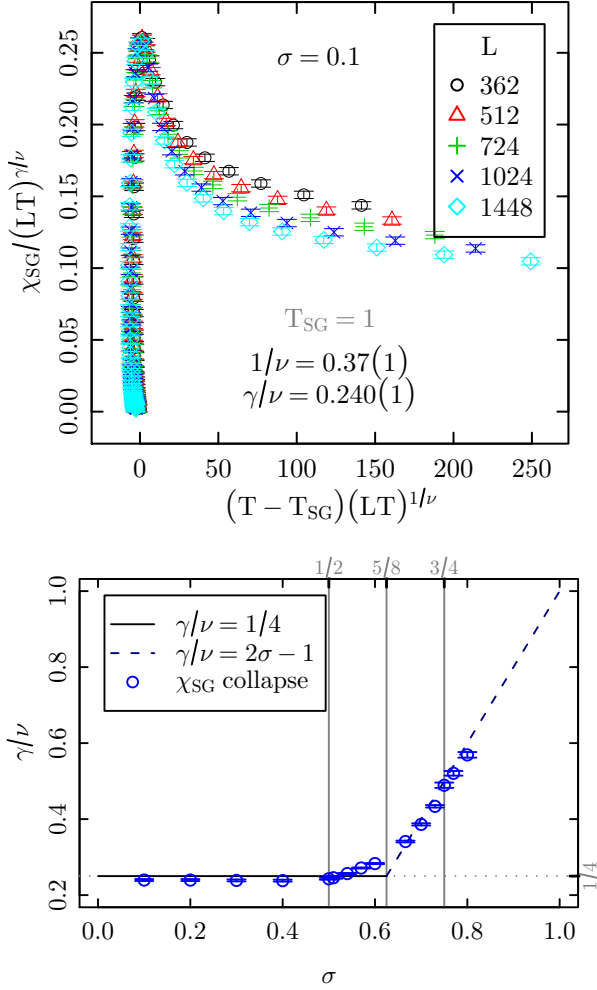


FIG. 27. (Color online). Top: A collapse of  $\chi_{SG}$  according to the extended scaling form (112) for  $\sigma = 0.1$  with adaptively determined parameters  $\gamma/\nu = 0.24$  and  $\nu = 0.37$  ( $T_{SG} = 1$ ). Bottom: estimates of  $\gamma/\nu$  resulting from an adaptive collapsing routine together with the theoretical expectations  $\gamma/\nu = 0.25$  for  $\sigma \leq 5/8$  and  $\sigma/\nu = 2\sigma - 1$  for  $\sigma > 5/8$ , respectively.

ences which are, in part, related to the shift in the lower and upper critical dimensions of the model.

The lack of metastability in the model allows to perform quasi-exact ground-state calculations. The resulting defect energies are well described by a long-range stiffness exponent  $\theta = 3/4 - \sigma$ . This relation can also be deduced from scaling arguments, but we have not been able to provide a more rigorous derivation. This relation results in an upper critical  $\sigma_u = 3/4$ , where finite-temperature spin-glass transitions first disappear. On lowering  $\sigma$ , mean-field behavior sets in at  $\sigma_l = 5/8$ . These critical interaction ranges are different from the  $\sigma_l = 2/3$  and  $\sigma_u = 1$  found for spin glasses with finite  $m$ .<sup>17</sup> For hypercubic lattices it has been speculated that  $d_l = d_u$  if  $m \rightarrow \infty$ .<sup>14,15</sup> According to our analysis of the 1d model theoretical as well as numerical evidence exists

showing that the upper and lower critical  $\sigma$  are well separated. We also investigated the distribution of ground-state energies, and it is found to be Gaussian for the full range of  $\sigma$ , again in contrast to the Ising case where non-Gaussian distributions were found in the mean-field regime<sup>20</sup>. Sample-to-sample fluctuations are trivial with  $\Theta_f = 1/2$  for  $\sigma > 1/2$ , but cross over to a value consistent with  $\Theta_f = 1/5$  for  $\sigma < 1/2$  as conjectured for the SK model in Ref. 63.

In Ref. 26 it has been suggested to study a diluted version of the 1d long-range spin-glass model to reach even larger system sizes. As we point out here, however, the two models are not in the same universality class for  $\sigma > 1$ , where the diluted model becomes equivalent to a short-range 1d system. Right at  $\sigma = 1$ , critical exponents depend continuously on the average coordination number  $z$ . Also, sample-to-sample fluctuations are trivial for the diluted model with  $\Theta_f = 1/2$  for *all*  $\sigma$ , an effect anticipated for the Ising case<sup>62</sup>. Additionally, we observe more pronounced scaling corrections for the diluted model even in the regime  $1/2 \leq \sigma \leq 1$  such that we cannot find an advantage for numerical simulations in the larger system sizes reachable through the dilution. Additionally, we compared different realizations of the 1d geometry using rings and chains with and without Ewald summation of interactions. As scaling corrections for this class of models are pronounced, one could hope that some variant of the model leads to a substantial reduction in corrections. For zero temperature (cf. Fig. 8) as well as for the critical behavior at  $T > 0$ , however, we find no significant differences in the FSS of the different model variants considered, cf. the data collected in Table IV.

The ground-state calculations are complemented by results from an iterative solution of the saddle-point equations resulting in the  $m \rightarrow \infty$  limit, yielding access to the order parameter, spin-glass susceptibility and correlation length. In contrast to Ref. 15, we argue that using appropriate definitions of the basic observables the model does show true long-range order in the low-temperature phase, even for the order of limits  $m \rightarrow \infty$  before  $N \rightarrow \infty$  naturally taken in numerical studies. The critical exponents  $\nu$ ,  $\beta$  and  $\gamma$  numerically determined from this approach are consistent with our theoretical arguments in the full range of  $\sigma$ . The critical exponents in the non-mean-field regime have been hard to determine with precision. However, one of the surprises is the utility of the simple approximate RG scheme first suggested by McMillan<sup>47</sup> which seems to work quite well over the entire non-mean field region,  $5/8 < \sigma \leq 3/4$ .

As an aside, we find clear-cut evidence of the recently suggested exactness of mean-field theory for spin-glass models in the regime  $\sigma < 1/2$ ,<sup>30</sup> where we see non-universal properties such as the average ground-state energy to be independent of the interaction range  $\sigma$ .

The  $m \rightarrow \infty$  model studied in this paper is an interesting model in its own right, partly because it is one of relatively few models known which have a failure of hyperscaling. The phenomenon of dimensional reduction

occurs in its short-range  $d$ -dimensional version which suggests that there might be some elegant supersymmetry in the model, but this has yet to be discovered. But our chief motivation in understanding this model was to clear the ground for our future  $1/m$  expansion study of spin glasses.

## ACKNOWLEDGMENTS

The authors are indebted to T. Aspelmeier, H. Katzgraber and A. P. Young for useful discussions. We thank T. Yavorskii for useful advice regarding the Ewald summation technique. The authors acknowledge computer time provided by NIC Jülich under grant No. hnz18 and funding by the DFG through the Emmy Noether Program under contract No. WE4425/1-1.

- 
- \* beyerf@uni-mainz.de  
† martin.weigel@coventry.ac.uk  
‡ m.a.moore@manchester.ac.uk
- <sup>1</sup> K. Binder and A. P. Young, Rev. Mod. Phys. **58**, 801 (1986).
  - <sup>2</sup> N. Kawashima and H. Rieger, in *Frustrated Spin Systems*, edited by H. T. Diep (World Scientific, Singapore, 2005) Chap. 9, p. 491.
  - <sup>3</sup> G. Parisi, Phys. Rev. Lett. **43**, 1754 (1979); **50**, 1946 (1983).
  - <sup>4</sup> M. A. Moore and A. J. Bray, Phys. Rev. B **83**, 224408 (2011).
  - <sup>5</sup> D. Sherrington and S. Kirkpatrick, Phys. Rev. Lett. **35**, 1792 (1975).
  - <sup>6</sup> T. Aspelmeier and M. A. Moore, Phys. Rev. Lett. **92**, 077201 (2004).
  - <sup>7</sup> J. R. L. de Almeida, R. C. Jones, J. M. Kosterlitz, and D. J. Thouless, J. Phys. C **11**, L871 (1978).
  - <sup>8</sup> A. J. Bray and M. A. Moore, J. Phys. C **14**, 2629 (1981).
  - <sup>9</sup> B. W. Morris, S. G. Colborne, M. A. Moore, A. J. Bray, and J. Canisius, J. Phys. C **19**, 1157 (1986).
  - <sup>10</sup> A. J. Bray and M. A. Moore, J. Phys. C **15**, L765 (1982).
  - <sup>11</sup> J. E. Green, A. J. Bray, and M. A. Moore, J. Phys. A **15**, 2307 (1982).
  - <sup>12</sup> L. W. Lee and A. P. Young, Phys. Rev. E **72**, 036124 (2005).
  - <sup>13</sup> F. Beyer and M. Weigel, Comp. Phys. Commun. **182**, 1883 (2011).
  - <sup>14</sup> L. Viana, J. Phys. A **21**, 803 (1988).
  - <sup>15</sup> L. W. Lee, A. Dhar, and A. P. Young, Phys. Rev. E **71**, 036146 (2005).
  - <sup>16</sup> F. J. Dyson, Commun. Math. Phys. **12**, 91 (1969); **21**, 269 (1971).
  - <sup>17</sup> G. Kotliar, P. W. Anderson, and D. L. Stein, Phys. Rev. B **27**, 602 (1983).
  - <sup>18</sup> A. J. Bray, M. A. Moore, and A. P. Young, Phys. Rev. Lett. **56**, 2641 (1986).
  - <sup>19</sup> H. G. Katzgraber and A. P. Young, Phys. Rev. B **67**, 134410 (2003).
  - <sup>20</sup> H. G. Katzgraber, M. Körner, F. Liers, M. Jünger, and A. K. Hartmann, Phys. Rev. B **72**, 094421 (2005).
  - <sup>21</sup> H. G. Katzgraber and A. P. Young, Phys. Rev. B **72**, 184416 (2005).
  - <sup>22</sup> R. S. Andrist, D. Larson, and H. G. Katzgraber, Phys. Rev. E **83**, 030106 (2011).
  - <sup>23</sup> A. Matsuda, M. Nakamura, and H. Kawamura, J. Phys.: Cond. Matt. **19**, 145220 (2007).
  - <sup>24</sup> D. X. Viet and H. Kawamura, Phys. Rev. Lett. **105**, 097206 (2010).
  - <sup>25</sup> A. Sharma and A. P. Young, Phys. Rev. B **83**, 214405 (2011); **84**, 014428 (2011).
  - <sup>26</sup> L. Leuzzi, G. Parisi, F. Ricci-Tersenghi, and J. J. Ruiz-Lorenzo, Phys. Rev. Lett. **101**, 107203 (2008).
  - <sup>27</sup> H. G. Katzgraber, D. Larson, and A. P. Young, Phys. Rev. Lett. **102**, 177205 (2009).
  - <sup>28</sup> L. Leuzzi, G. Parisi, F. Ricci-Tersenghi, and J. J. Ruiz-Lorenzo, Phys. Rev. Lett. **103**, 267201 (2009).
  - <sup>29</sup> L. Leuzzi, J. Phys. A **32**, 1417 (1999).
  - <sup>30</sup> T. Mori, Phys. Rev. E **84**, 031128 (2011).
  - <sup>31</sup> W. H. Press, S. A. Teukolsky, W. T. Vetterling, and B. P. Flannery, *Numerical Recipes: The Art of Scientific Computing*, 3rd ed. (Cambridge University Press, Cambridge, 2007).
  - <sup>32</sup> D. Larson, H. G. Katzgraber, M. A. Moore, and A. P. Young, Phys. Rev. B **81**, 064415 (2010), arXiv:0908.2224.
  - <sup>33</sup> L. Viana and A. J. Bray, J. Phys. C **18**, 3037 (1985).
  - <sup>34</sup> R. N. Bhatt and A. P. Young, J. Magn. Magn. Mater. **54-57**, 191 (1986).
  - <sup>35</sup> M. Abramowitz and I. A. Stegun, *Handbook of Mathematical Functions: with Formulas, Graphs, and Mathematical Tables*, 1st ed., Dover books on mathematics (Dover Publications, 1965).
  - <sup>36</sup> J. J. Alonso and J. F. Fernández, Phys. Rev. B **81**, 064408 (2010).
  - <sup>37</sup> V. Privman, in *Finite Size Scaling and Numerical Simulation of Statistical Systems*, edited by V. Privman (World Scientific, Singapore, 1990) pp. 1–98.
  - <sup>38</sup> K. Binder, Z. Phys. B **61**, 13 (1985).
  - <sup>39</sup> J. L. Jones and A. P. Young, Phys. Rev. B **71**, 174438 (2005).
  - <sup>40</sup> D. S. Fisher and D. A. Huse, Phys. Rev. B **38**, 386 (1988).
  - <sup>41</sup> M. A. Moore, Phys. Rev. B **82**, 014417 (2010).
  - <sup>42</sup> A. C. D. van Enter and J. L. van Hemmen, J. Stat. Phys. **39**, 1 (1985).
  - <sup>43</sup> G. Stell, Phys. Rev. B **5**, 981 (1972).
  - <sup>44</sup> M. Suzuki, Prog. Theor. Phys. **49**, 424 (1973).
  - <sup>45</sup> M. E. Fisher, S. K. Ma, and B. G. Nickel, Phys. Rev. Lett. **29**, 917 (1972).
  - <sup>46</sup> T. Aspelmeier, M. A. Moore, and A. P. Young, Phys. Rev. Lett. **90**, 127202 (2003).
  - <sup>47</sup> W. L. McMillan, Phys. Rev. B **29**, 4026 (1984).
  - <sup>48</sup> A. J. Bray and M. A. Moore, in *Heidelberg Colloquium on Glassy Dynamics*, edited by J. L. van Hemmen and I. Morgenstern (Springer, Heidelberg, 1987) p. 121.
  - <sup>49</sup> F. Barahona, J. Phys. A **15**, 3241 (1982).
  - <sup>50</sup> M. B. Hastings, J. Stat. Phys. **99**, 171 (2000).
  - <sup>51</sup> S. Chandra, Phys. Rev. E **77**, 021125 (2008).
  - <sup>52</sup> I. Campos, M. Cotallo-Aban, V. Martín-Mayor, S. Perez-

- Gaviro, and A. Tarancón, Phys. Rev. Lett. **97**, 217204 (2006).
- <sup>53</sup> J. P. Bouchaud, F. Krzakala, and O. C. Martin, Phys. Rev. B **68**, 224404 (2003).
- <sup>54</sup> I. A. Campbell, A. K. Hartmann, and H. G. Katzgraber, Phys. Rev. B **70**, 054429 (2004).
- <sup>55</sup> S. Boettcher and S. Falkner, (2011), preprint 1110.6242, arXiv:1110.6242.
- <sup>56</sup> S. Boettcher, Eur. Phys. J. B **74**, 363 (2010).
- <sup>57</sup> T. Aspelmeier, A. Billoire, E. Marinari, and M. A. Moore, J. Phys. A **41**, 324008 (2008).
- <sup>58</sup> A. Braun and T. Aspelmeier, Phys. Rev. B **74**, 144205 (2006).
- <sup>59</sup> A. Andreanov, F. Barbieri, and O. C. Martin, Eur. Phys. J. B **41**, 365 (2004).
- <sup>60</sup> S. Boettcher, Eur. Phys. J. B **46**, 501 (2005).
- <sup>61</sup> G. Parisi and T. Rizzo, Phys. Rev. B **79**, 134205 (2009).
- <sup>62</sup> G. Parisi and T. Rizzo, J. Phys. A **43**, 045001 (2010).
- <sup>63</sup> T. Aspelmeier and A. Braun, Phys. Rev. B **81**, 094439 (2010).
- <sup>64</sup> I. Kondor, J. Phys. A **16**, L127 (1983).
- <sup>65</sup> J. R. Banavar and M. Cieplak, Phys. Rev. Lett. **48**, 832 (1982).
- <sup>66</sup> A. J. Bray and M. A. Moore, J. Phys. C **17**, L463 (1984).
- <sup>67</sup> J. M. Kosterlitz and N. Akino, Phys. Rev. Lett. **82**, 4094 (1999).
- <sup>68</sup> M. Weigel and M. J. P. Gingras, Phys. Rev. Lett. **96**, 097206 (2006).
- <sup>69</sup> M. Weigel and M. J. P. Gingras, Phys. Rev. B **77**, 104437 (2008).
- <sup>70</sup> L. S. Schulman, J. Phys. A **16**, L639 (1983).
- <sup>71</sup> C. M. Newman and L. S. Schulman, Commun. Math. Phys. **104**, 547 (1986).
- <sup>72</sup> I. Benjamini and N. Berger, Random Struct. Alg. **19**, 102 (2001).
- <sup>73</sup> R. Juhász, Phys. Rev. E **85**, 011118 (2012).
- <sup>74</sup> B. Efron and R. J. Tibshirani, *An Introduction to the Bootstrap* (Chapman and Hall, Boca Raton, 1994).
- <sup>75</sup> H. G. Ballesteros, A. Cruz, L. A. Fernández, V. Martín-Mayor, J. Pech, J. J. Ruiz-Lorenzo, A. Tarancón, P. Téllez, C. L. Ullod, and C. Ungil, Phys. Rev. B **62**, 14237 (2000).
- <sup>76</sup> J. Houdayer and A. K. Hartmann, Phys. Rev. B **70**, 014418 (2004).
- <sup>77</sup> S. M. Bhattacharjee and F. Seno, J. Phys. A **34**, 6375 (2001).
- <sup>78</sup> I. A. Campbell, K. Hukushima, and H. Takayama, Phys. Rev. Lett. **97**, 117202 (2006).
- <sup>79</sup> H. G. Katzgraber, M. Körner, and A. P. Young, Phys. Rev. B **73**, 224432 (2006).